AN ABSTRACT OF THE THESIS OF

Lance Changyong Kim for the degree of Master of Science in Chemical Engineering presented on May 24, 1995. Title: A Parametric Study of the Design of Coathanger Dies using Computational Fluid Dynamics.

Redacted for Privacy

Abstract Approved : _____

Willie E. (Skip) Rochefort

A Computational Fluid Dynamics (CFD) approach has been used to perform a parametric study to design a coathanger die for power-law fluids. The initial motivation for the work was to design a film die for the production of high performance thin films from a lyotropic liquid crystal polymer system, poly (*p*-phenylene-cis-benzobisoxazole) in polyphosphoric acid (PBO/PPA). The rheological properties of the PBO/PPA system are: high viscosity at low shear rate, and highly non-Newtonian, shear-thinning behavior which can be described by the power-law model with a low value of the power-law index (n= 0.1 - 0.2) over the shear rate range of interest in the commercial film die. The main purpose of the thesis work was to examine the key parameters which affect the die geometry and outline a general method of die design for coathanger dies with power-law fluids. A commercially available CFD program (FLUENT), which could be of general use in an industrial setting, was chosen for this purpose.

The die design chosen for the parametric study was the linearly tapered coathanger die with a teardrop cross-section in the manifold region. This is

one of the most prevalent commercial film die designs. The film die dimensions were chosen to match those of a laboratory film die used for the PBO/PPA system. The key dimensions are: inlet pipe length = 0.06 m and radius = 0.005 m.; initial radius (R_o) of the manifold = 0.005 m; teardrop angle = 60 °; prelanding zone height (H_1) = 0.002 m.; landing zone height (H_2) = 0.001 m.; die width (W) = 0.2 m. Based on previous analytical work by Chung and Lohkamp (1976), the main independent parameters studied were inlet velocity (or flow rate), length of the landing zone (L), and manifold angle (θ). The primary criteria performance used in this study was uniform film thickness at the die exit (i.e., uniform flow rate across the width). The modeling results show that the film thickness uniformity is not strongly effected by inlet flow rate, but can be optimized as a function of manifold angle after determining the asymptotic region for the length of landing zone. The asymptotic region for the landing zone length is defined, in this study, as that length beyond which "entrance effects" are no longer significant. These entrance effects are a function of the length of prelanding zone, which is determined from the manifold angle (θ). Therefore, in practice the designer would typically determine the landing zone length based on criteria such as maximum allowable pressure drop through the die, then use the method outlined in this thesis to select the preferred manifold angle (θ), using uniform film thickness at the die exit as the performance criteria. The preferred manifold angle for a coathanger film die designed for the PBO/PPA system was θ = 65°, using landing zone length L = 0.05 m; inlet flow rate = 3.9270 m^3 / sec; power-law model parameters K = 10000 $Pa \cdot \sec$ and n = 0.12. It was determined that the preferred geometry was not very sensitive to the magnitude of the viscosity or to the power-law index for values of n > 0.5. However, for highly non-Newtonian fluids (n= 0.1 - 0.2) such as the

PBO/PPA system, the flow distribution at the die exit was *very sensitive* to manifold angle. The obvious extension of these studies is to rheological models which incorporate elasticity and/or yield stress phenomena in the fluid constitutive equation.

A Parametric Study of the Design of Coathanger Dies using Computational Fluid Dynamics

By

Lance Changyong Kim

A THESIS

submitted to

Oregon State University

in partial fulfillment of
the requirements for the
degree of

Master of Science

Completed May 24, 1995
Commencement June 1996

Master of Science thesis of Lance Changyong Kim presented on May 24, 1995

APPROVED:

Redacted for Privacy

Major Professor, representing Chemical Engineering

Redacted for Privacy

Chair of Department of Chemical Engineering

Redacted for Privacy

Dean of Graduate School

I understand that my thesis will become part of the permanent collection of Oregon State University libraries. My signature below authorizes release of my thesis to any reader upon request.

Redacted for Privacy

Lance Changyong Kim, Author

ACKNOWLEDGMENT

I would like to acknowledge the guidance and help provided by my advisor, Dr. Skip Rochefort throughout my studies. Special thanks are due to Jeff McKinnis and other colleagues of my department.

Special acknowledgment is extended to my friends and relatives in Korea for their encouragement and support. A great debt of thanks is also due to all my friends in Corvallis. I would like to acknowledge emotional and financial support from my parents, my wife, and my son. Finally, I would like to thank the Lord God for his blessing.

TABLE OF CONTENTS

TABLE OF CONTENTS (CONTINUED)

LIST OF FIGURES

LIST OF FIGURES (continued)

LIST OF FIGURES (continued)

LIST OF FIGURES (continued)

LIST OF FIGURES (continued)

LIST OF APPENDIX FIGURES

LIST OF APPENDIX TABLES

NOMENCLATURE

H_1 = The height of the prelanding zone for a coathanger die, 0.002 m

H_2 = The height of the landing zone for a coathanger die, 0.001 m

K = The zero shear viscosity for a power-law fluid, $Pa \cdot \sec$

L = The length of the landing zone for a coathanger die, m

L_1 = The length of prelanding zone, m

n = The power-law index of a power-law fluids

$P(x)$ = The pressure along the x-axis, Pa

$P(z)$ = The pressure along the z-axis, Pa

ΔP_1 = The pressure drop over the prelanding zone, Pa

$Q(x)$ = The flow rate along the manifold, $m^3 / \sec$

$Q_\circ$ = The total flow rate, $m^3 / \sec$

$R(x)$ = The radius along the manifold, m

$R_\circ$ = The initial radius of the manifold for a coathanger die, 0.005 m

S = The flow rate per unit of a coathanger width, $m^3 / \sec$

T = The teperature of a system, $^\circ C$

w = The inlet velocity of a power-law fluid into a coathanger die, $m / \sec$

W = The die width of a coathanger die, 0.2 m

Greek Letters

α = Underrelaxation factor,

η = Viscosity, $Pa \cdot \sec$

θ = The manifold angle of a coathanger die, degree

NOMENCLATURE (continued)

ϕ = The conserved quantity of the equations for the conservation of mass, momentum, energy and chemical species

ϕ_N = The new value of a variable is calculated upon the old value at a node point

$\Delta\phi$ = The computed change in ϕ_N

A Parametric Study of the Design of Coathanger Dies using Computational Fluid Dynamics

INTRODUCTION

The major goal in the design of film dies is to obtain the optimal die geometry to produce polymer film of uniform thickness with the least amount of adjustment of the choker bar or die lip (Figure 2.1). In order to produce wide film of uniform thickness, an even flow rate in the exit region of the die channel must be obtained. To this end, the main result of the present study is the outline of a procedure to determine the preferred design of a coathanger die when a power-law constitutive model can be used to describe the fluid behavior. This design procedure is described such that it can be applied in a general manner to industrial film die design.

The goals of the studies presented in this thesis are really twofold. The first, and more general goal, was to use a Computational Fluid Dynamics (CFD) package to develop a three dimensional (3-D) model for the design of a coathanger extrusion die for the production of polymer film or sheet from high viscosity, highly non-Newtonian fluids that exhibit power-law behavior. The commercial CFD packages available have been used extensively for 2-D simulations of these types of flows, but 3-D simulations are much less prevalent, and most often relegated to simple Newtonian fluids. There are no previous studies to show a general procedure to determine the optimal film die geometry developing 3-D model. The second, and more specific goal, was to apply the techniques developed to the design of a film die for the processing of a Lyotropic Liquid Crystal Polymer (LLCP), for which both

rheological and processing data were available from previous studies (Ernst et al., 1992).

There are basically three types of approaches which can be used for the design of film dies. The first is to use an analytical solution to a simplified model of the flow, usually in only one or two dimensions. This type of approach has typically been done using the classical lubrication theory. A second approach is to do the experimental work in a laboratory using trial and error parametric studies. As one might expect, this method is both costly and time consuming - and not always practical. The third method is to do a computer simulation using commercially available CFD programs. This is most assuredly the method of choice in industry, primarily due to time and cost savings, as well as flexibility. It is certainly more desirable to run twenty simulations and build one or two prototype dies, than to build many prototype dies. There are a number of commercial CFD packages available for the solution of general fluid mechanics problems. They generally employ either finite difference or finite element techniques and are sufficiently general to work for a wide range of problems (i.e., gases or liquids in laminar or turbulent flow with varying geometries). However, most of these programs have also been developed to meet the needs of a particular market, be it aerospace or polymer processing, so that there is usually some "built-in" specialization to the packages - problems that they are best suited to handle. The CFD package that has been used in this study is FLUENT (Fluent Inc., Lebanon, N.H.), a very general program which can handle problems ranging from gas flow and diffusion in low pressure CVD reactors to polymer processing operations.

As was mentioned earlier, beyond the general goal of designing the die geometry for a highly non-Newtonian fluid, the particular case of interest was

the Lyotropic Liquid Crystal Polymer (LLCP) system of 14 wt% solution of poly(*p*-phenylene-cis-benzobisoxazole) in polyphosphoric acid (PBO/PPA). The 14wt% solution of PBO/PPA is a highly non-Newtonian (shear thinning) polymeric fluid which can be represented by a power-law fluid model. The major assumption in this scenario is that the polymer fluid is highly viscous but not very elastic. It has been observed that many liquid crystal polymer systems show just this type of behavior. They are highly viscous and extremely non-Newtonian (shear thinning) but exhibit very little elastic behavior, as would be measured in a standard extrudate swell experiment. This is not unexpected, as the mechanisms responsible for large extrudate swell are molecular entanglements , and entanglements are minimized in the highly aligned, rigid polymer systems. Therefore, the use of a power-law model for the production of thin films from liquid crystal polymers appears to be a reasonable assumption.

In order to perform a simulation to arrive at the preferred die design for a particular non-Newtonian fluid, the key geometric parameters must be identified. An equation which was derived mathematically by Chung and Lohkamp (1976) was used to choose the parameters. This equation is described in more detail in Chapter 3 and Appendix 3. On the basis of this equation, there appear to be three independent parameters of primary importance to determine the preferred geometry of a film die (Figure 3.7). Those independent parameters are manifold angle θ, inlet velocity (or flow rate) w, and length of landing zone L. Other parameters such as die width W , initial radius of manifold R_o, height of prelanding zone H_1, and height of landing zone H_2 are dependent variables to manifold angle θ.

Using a Computational Fluid Dynamics (CFD) package (FLUENT), the geometry effects on a coathanger die were studied to optimize the film die

design according to the parameters suggested by the Chung and Lohkamp model (1976). The optimized geometry of the coathanger die was then tested for various power-law fluids of increasing non-Newtonian character.

CHAPTER 2 : LITERATURE REVIEW

The earliest film die designs described a converging-diverging channel with an adjustable die lip. This particular design provided a smooth flow path, but it did not lead to the uniform distribution of flow. The main problem is that the die is typically fed by an extruder through a circular, small (relative to the width of the film) opening at one end of the die (back, side, or bottom fed). Somehow, the polymer must be uniformly distributed over the width of the die so that the exiting film (which may be a wide as several meters in some cases), leaves the die lips thermally homogeneous and with a uniform stress distribution. The history through the die can lead to a non-uniform stress distribution, which in turns gives a non-uniform thickness profile at the die exit. Once again, it should be noted that the stated objective in film die design is always uniform flow rate across the die lip, which for a uniform cross-section die will lead to uniform film thickness. While the flow of a molten polymer or polymer solution in a film die is three dimensional in nature, mainly simplified approaches (1-D or 2-D) have been used for the purpose of die design. It has been known for many years that control of manifold geometry is critical for uniform flow distribution across the film width.

Pearson [1964], McKelvey and Ito [1971] studied the flow distribution problems in a T-die, the geometry of which is shown in Figure 2.1 (a). The T-die generally does not satisfy the requirement of uniform flow distribution across the die width and is known to develop " dead spots" (stagnant regions) in the corners of the manifold region. The abrupt transitions in the entry region and manifold exit region also cause problems. Both authors suggested

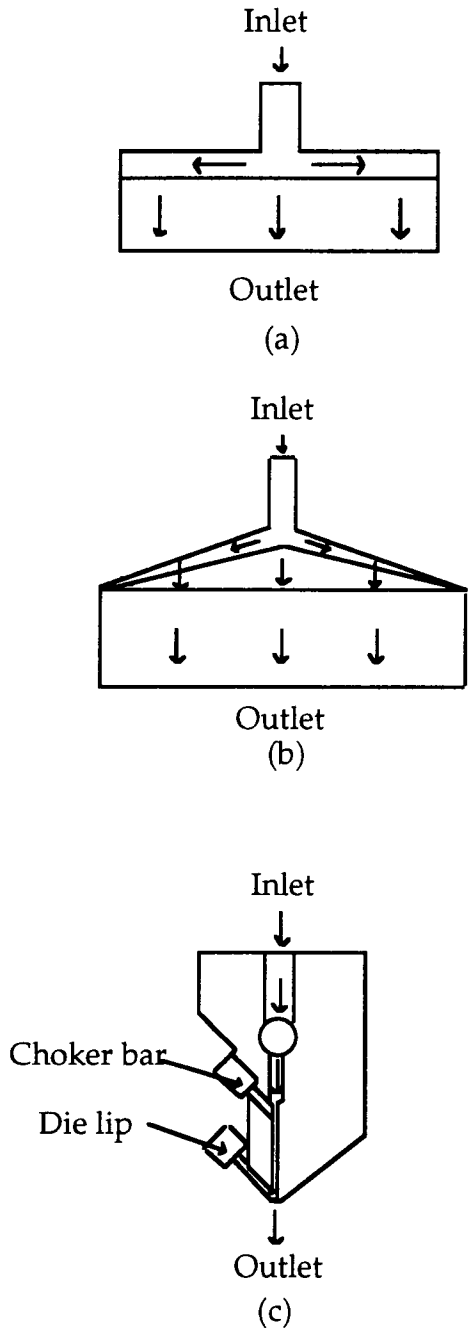

Figure 2.1 (a) T-die (Top view) (b) Coathanger die (Top view) (c) Coathanger die (Side view)

a tapered manifold and a tapered die land joining the manifold to the die lip in order to obtain a uniform flow rate along the die width.

The coathanger die, as shown in Figure 2.1 (b), was studied later by Chung and Lohkamp [1976], Matsubara [1979, 1980, 1983], Winter and Fritz [1986], and Liu, Hong, and Chen [1988]. These studies typically involved mathematical derivations of the governing flow equations in one or two dimensions with simplifying assumptions and simple constitutive equations for the polymer.

Chung and Lohkamp [1976] derived equations for the optimum geometry of the manifold section, coathanger section, and die-lip section and for uniform flow rate distribution at the die exit, for the 1-D flow case with several severe limiting assumptions. This will be discussed in greater detail in a later section. They showed how the initial inlet radius of the manifold depends on manifold angle, channel width, coathanger gap, and power-law index, n. Finally, they concluded that the manifold profile depends only on the shear sensitivity of the polymer melt, and nothing else. The geometry of their film die is given in Figure 2.1 (c).

Matsubara [1979, 1980, 1983] provided an approximate method of geometry design of a coathanger die having both uniform flow rate and residence time across the full width of the die for an isothermal, power-law fluid. In this study he used almost the same assumptions (isothermal power-law fluids, ideally designed manifold having the even flow rates from the manifold into the coathanger section, two flow components inside the flow channel, and circular tube manifold) with which Chung and Lohkamp [1976] derived their model. But he also derived equations for the residence time distribution in the coathanger die. The residence time distribution of the die is important when one tries to produce film using a polymer which can be

degraded after passing a certain amount of time at high temperature inside the die.

Winter and Fritz [1986] studied a rectangular cross-section instead of a circular cross-section for the manifold. They suggested that the cross-section of the manifold need not be circular.

Liu, Hong, and Chen [1988] studied the development of a code to analyze a linearly-tapered coathanger die. They derived the general governing equation for flow distribution inside the die with some limiting assumptions (isothermal system, power-law fluids, flow to the machine direction only in the landing zone, no entrance effect, no end effect, etc.). On the basis of this equation, they developed the design formula for a die to deliver uniform flow. They also examined the variations of lateral flow uniformities and residence time distributions of polymeric liquids under several different design and operating conditions, using manifolds with non-circular cross-sections, adjusting production widths, and delivering fluids with different viscosities.

These above studies were based on the classical lubrication theory, which assumes that one velocity component and one gradient are dominant in the flow domain of a model geometry. And the most of them were tried to derive mathematical equations theoretically using hand calculation without using CFD programs.

For this reason, a different approach was used by Vergnes, Saillard, and Agassant [1984], employing a finite difference method to solve the 2-D flow field in the die based on the assumption of a narrow flow channel for the non-isothermal flow of a power-law fluid in a coathanger geometry. Although they considered thermal regulation in detail, they did not

investigate the effect of flow channel geometry, which is of fundamental importance.

In recent years there has been an increasing interest in the use of the finite element or finite difference methods in polymer processing problems because of the potential to deal with the complicated geometries, boundary conditions, and fluids properties.

Lee, Wen, and Liu [1990] studied vortex formation in a dual-cavity coathanger die. They showed the effects of cavity shapes and the rheological properties of the polymeric liquids on the vortex formation (dead spots) in cavities using a flow visualization technique, but they did not provide any modeling.

Wang [1991] studied the isothermal power-law flow in slit dies and coathanger dies. He realized that both the design of the geometry for the manifold and channel cross-section were needed to obtain uniform flow rate distributions. Since the flow channel consists of varying cross-sections, he needed to employ a three-dimensional analysis, which not only provides the data of flow uniformity, but also yields detailed information of the flow field which, for instance, will help identify flow irregularities such as dead spots. He ignored melt elasticity, assuming that a coathanger die with smoothly varying cross-sections will minimize the elastic effects which are most prevalent in situations involving sudden contractions. The pressure, velocity, distribution, and transverse flow rate distributions were all obtained. The effect of the die geometry on flow distribution was critical. He showed the flow rate distributions for several geometries with a power-law fluid. However, he did not find the optimal geometry for the model or consider the effects of other parameters (inlet flow rate, length of landing zone, power-law index n, etc.) on the flow rate distributions. Finally, he suggested that an

iterative approach would be required in order to define the details of die geometry.

Arpin, Lafleur, and Sanschagrin [1994] studied coathanger die design using a computer software program. They developed a program which is able to run on a personal computer (PC) with only a few minutes of calculation time. However, they developed a code only for the 2-D geometry, without finding the optimal geometry for the production of uniform HDPE and LLDPE films which were of interest to them.

While the previous work on film die design covered a broad range of issues concerning analytical solutions of 1-D and 2-D models, and in a few cases 3-D simulations using commercial software packages, there are really no studies which combined the issues to outline a path for the preferred design for the coathanger die geometry which could be easily implemented in an industrial setting. This provided the motivation for the present studies, in which a commercially available CFD program was used to arrive at an optimal manifold die geometry for a power-law fluid with highly non-Newtonian behavior.

CHAPTER 3 : MODELING METHODS AND CONDITIONS

3.1 FLUENT

In the past ten to fifteen years there has been a major increase in the number of Computational Fluid Dynamics (CFD) packages commercially available. It is no longer necessary for the researcher to undertake the relatively large task of writing a computer code from the ground up. Instead, the challenge is now to identify the CFD package which best fits the problems to be solved. Some codes are highly specialized, either for particular types of problems (i.e., coating flows; air foil design; extruder or die design) or particular fluids (gases and liquids; non-Newtonian polymer melts; etc.). The advantage of these specialized codes are typically ease of use and very fast "up-time". The disadvantage, of course, is flexibility in the types of problems that can be solved. There are also a number of very general CFD codes available which work on several different types of problems, with many different types of fluids. However, even with these generalized CFD packages, there is typically an inherent bias towards a particular class of problems. For instance, many CFD packages can handle laminar and turbulent flows of gases and liquids, but are not very efficient for viscous, non-Newtonian flows of polymer melts. Those which are particularly suited to solving polymer processing problems generally cannot handle turbulent mixing of gases very well. Therefore, the selection of the CFD package follows some very simple guidelines:

(1) A general package which is best suited for the primary area of research interest

(2) Fast start-up time to become a fairly proficient user.

(3) User friendly interface and flexible data presentation format.

(4) Ease of manipulation of geometries, grid generation, and data input.

(5) Cost.

These issues all played some part in the selection of the CFD package used in these studies and described in some detail in the following sections.

FLUENT is one of the most widely used Computational Fluid Dynamics (CFD) programs for modeling fluid flow, heat transfer, mass transfer and chemical reactions. It's basic program capabilities are given below: steady state or transient flow; incompressible or compressible flow; laminar or turbulent flow; coupled conduction/convection heat transfer (including both free and forced convection); radiational heat transfer; mixing of chemical species; reaction of chemical species; temperature and composition dependent fluid/material properties; flow through porous media; dispersed second phase particles/bubbles/droplets; ***laminar flow of non-Newtonian fluids (power-law model).***

In FLUENT, the equations for the conservation of mass, momentum, energy and chemical species are solved using a finite volume technique. In the finite volume technique, the governing equations are integrated over each control volume. This formulation ensures that all solutions satisfy the conservation equations, and provides solution stability and accuracy, particularly in the presence of strong gradients. FLUENT uses the finite difference method (FDM) as the numerical technique of the program.

3.2 Basic concepts of CFD programs

CFD programs generally consists of three basic modules, as depicted in Figure 3.1. The first module is the *pre-processing* module. In this module the model geometry is set-up, a grid is generated, and the data necessary to do the model calculation is supplied. Geometries are created in the following hierarchical fashion. *Points* are defined in terms of Cartesian coordinates. *Curves* are created from defining points. *Surfaces* are created from defining curves. Finally, *volumes* are created by connecting surfaces. Once each volume element is created, it is necessary to describe a boundary-type label that defines each element as a flow inlet, exit, solid boundary (wall), etc. After defining the geometry, a grid is generated based on curvilinear body-fitted coordinates (BFC). Using curvilinear body-fitted coordinates (BFC), the real geometry of the coathanger die described in Figure 3.3 is transformed to the geometry shown in Figure 4.1, which is used to do the calculations. Not all geometry descriptions will allow you to generate a structured body-fitted grid suitable for analysis in FLUENT. When you generate a body-fitted grid, the geometry is used to define the grid points on the geometric boundaries. Hence, when you are using a CFD program like FLUENT, the restrictions on the topology of the grid become restrictions on the topology of the geometry as well. The restrictions that arise are described in more detail below.

In a 2-D geometry as depicted in Figure 3.2 (a), the geometry must be topologically rectangular (four sided). Each of these four sides of the 2-D geometry (and of any internal geometric regions) must be represented by a separate edge curve (or group of curves). In a 3-D geometry, the restriction of structured six-sided control volumes is described as below. The geometry must have six-surfaces, like a brick, as shown in Figure 3.2(b). In addition, all

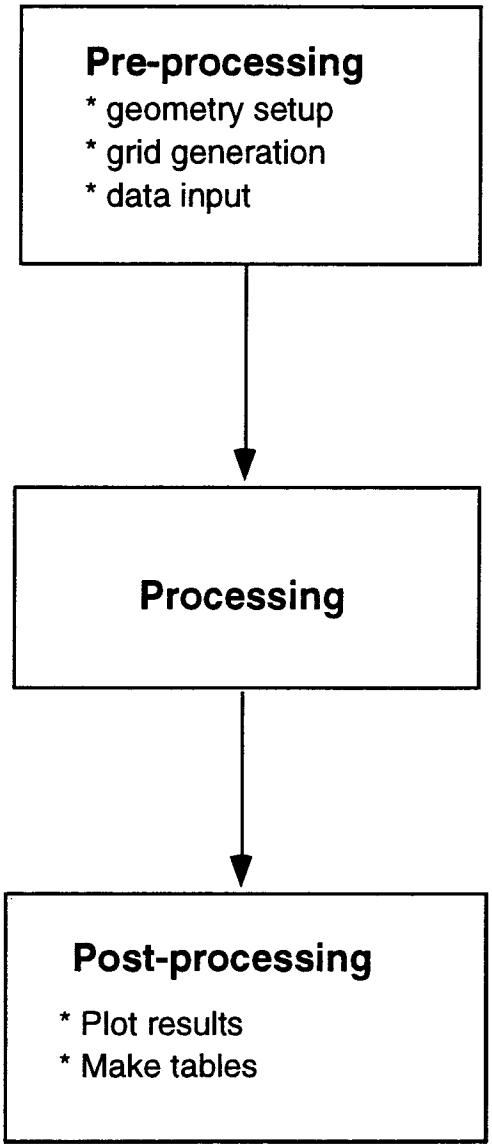

Figure 3.1 Computational Fluid Dynamics (CFD) Basic Program Structure

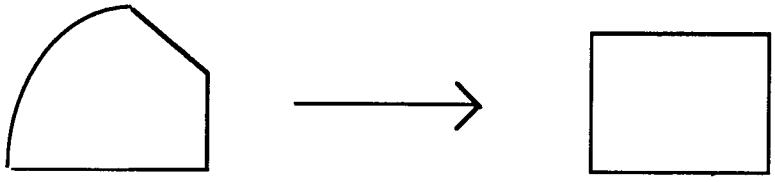

Topologically Rectangular Shape (Four-Sided)

(a)

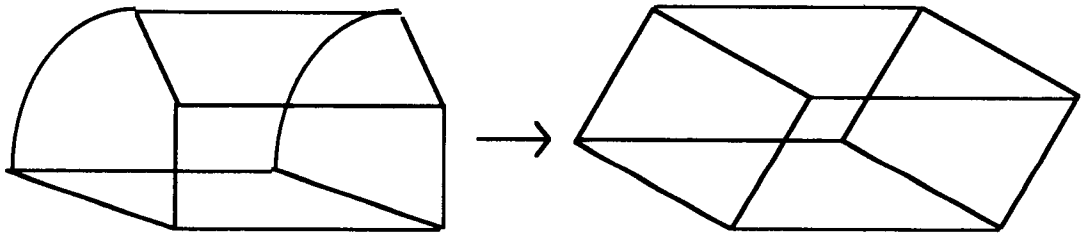

Topologically Hexahedral Shape (Six-Sided)

(b)

Figure 3.2 Topological geometry in FLUENT

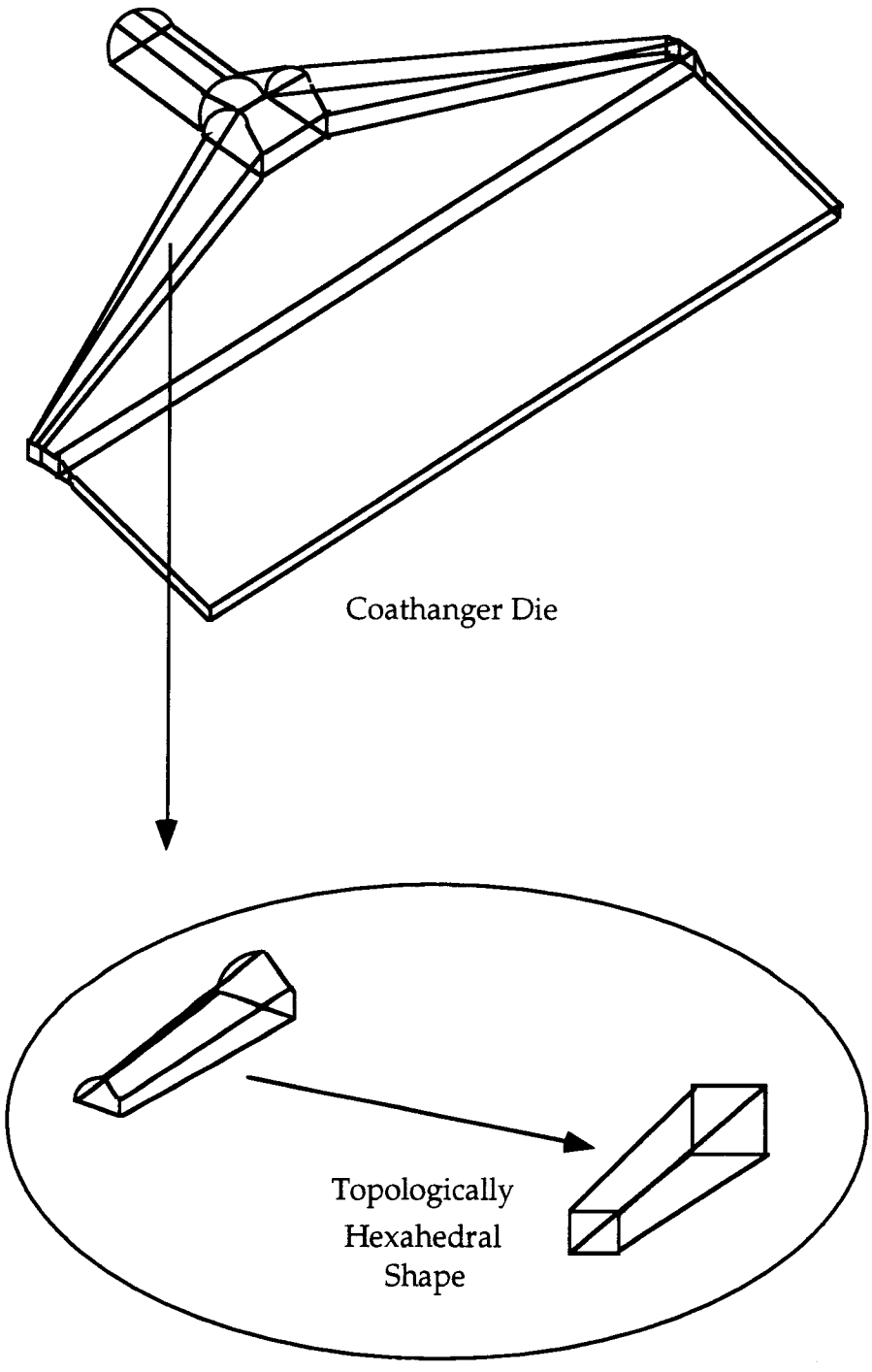

Figure 3.3 Topologically hexahedral shape of a segment volume of a coathanger die

surfaces contained in the geometry must be topologically rectangular (four-sided). The geometry description will effect the shape of the body-fitted grid that one can generate. To set up the geometry of a coathanger die in 3-D for example, one must consider the above restrictions. As shown in Figure 3.3, each segment of the entire volume of the coathanger die must be topologically six-sided (like a brick). The coathanger die grid generated consists of eight segment volumes, where each segment volume is topologically six-sided (six surfaces).

Geometry set-up and grid generation are the most time-consuming parts in many CFD analyses. Once the geometry and grid have been defined, the next step is data input. In this step the fluid properties are input (constitutive equation; for PBO/PPA solution, $\eta = K\dot{\gamma}^{n-1}$; $K = 10000\ Pa \cdot \sec$; n = 0.12), the boundary conditions (such as no slip condition; symmetry; inlet flow rate), and other parameters which are related to the convergence of the solution (such as underrelaxation parameter of each velocity component, pressure, temperature, viscosity, etc.) are specified.

The second module is the *processing* module. In this step the calculations are performed to see if there is a solution to the problem that has been posed. If the solution converges, then one may proceed to analysis of the results. When the solution diverges, then one must return to the *pre-processing* module to change some parameters which are related to solution convergence. These are discussed in the following section. Once the solution has converged, the final step is handled in the *post-processing* module. This module provides tools necessary to examine the results of the simulations. For example, one can make contour plots, vector plots, x-y coordinate plots, and tables that depict the velocity, pressure, temperature, viscosity, concentration, etc. at each node point in the 3-D space of the model.

3.3 Parameters which are related to speed of convergence

The way that the FLUENT program works is to solve the governing partial differential equations for conservation of mass, momentum, and energy by using a finite difference method to reduce the partial differential equations to a set of simultaneous algebraic equations.

The set of simultaneous algebraic equations are then solved using a Line-Gauss-Seidel (LGS) solver and performing the required number of iterations to get a convergent solution.

There are several factors which effect convergence, and in this section, the most important parameters with respect to the speed of convergence will be discussed. Complex flow properties, complex geometry, and a large number of computational cells are the three main reasons for slow convergence (or in some cases, divergence). Making an educated guess for the important flow variables is an excellent way to speed convergence. FLUENT uses zero as the default value for the initial guess of all of the variables throughout the domain. For complex fluid models, the most important technique for speeding convergence is to start from the simplest case. For example, to simulate a non-Newtonian fluid model, one should start from a Newtonian fluid model (n = 1.0). Once the solution for the Newtonian model is obtained, the solution can be directly used as the initial guess for the power-law model, starting with a power-law index n =0.9. Then, the solution for n =0.9 is used as the initial guess for the n =0.8 case, etc..Using this step by step approach, one can obtain the solutions for very shear thinning fluids with power-law indices as low as n =0.10, and not have a problem with divergence. If, for example, the same problem were run directly for n<0.5, then the solution

would either not converge or take a very large number of iterations to converge.

Another parameter which is related to convergence is the underrelaxation parameter, which is essentially a weighting factor. During each iteration, the new value of a variable is calculated upon the old value at a node point N. To calculate the new value, one has to multiply by the underrelaxation factor, α as below:

$$\phi_N = \phi_{N,old} + \alpha\Delta\phi \qquad \text{Equation 3.1}$$

ϕ is the conserved quantity of the equations for the conservation of mass, momentum, energy and chemical species. $\Delta\phi$ is the computed change in ϕ_N. The choice of the underrelaxation parameter is largely based upon experience, so that it is somewhat tricky to attempt to speed convergence by changing the value of underrelaxation parameter of each variable.

3.4 Liquid Crystal Polymers

The liquid crystal state is intermediate between that of a crystalline solid and an isotropic liquid, and as such possesses properties common to both. One can speak of order in liquid crystal polymers, but generally it is only one or two dimensional and on a local scale (domanial regions), not the three dimensional crystal lattice structure of true crystalline solids. Isotropic liquids have physical properties which are the same in all directions and can flow under an applied shear stress. Liquid crystal polymers flow under shear stress

but can have physical properties which are very directionally dependent, making them truly anisotropic in the liquid state.

There are two major classes of liquid crystal polymers, thermotropic and lyotropic. The thermotropic liquid crystal polymers (TLCPs) exhibit an anisotropic phase as a polymer melt and their transition from an anisotropic to isotropic state is driven by increasing temperature. For many of the main chain TLCPs with extremely stiff polymer backbones, the polymer degrades before it ever gets to an isotropic state. The second type of LCP is one in which the rigid polymer is dissolved in a solvent (usually a strong acid) and the anisotropic to isotropic phase transition is driven by a combination of concentration and, to a lesser extent, temperature. At low concentrations the solutions are isotropic, and as the concentration is raised the viscosity increases and reaches a maximum at some critical concentration, at which point the solution becomes birefringent, indicative of some degree of ordering in the system and the onset of liquid crystalline behavior. A phenomena which is often observed with lyotropic liquid crystalline polymers (LLCPs) is called "stir opalescence", in which the polymer solution is continuously being stirred while the concentration is increased until at some point the entire vessel becomes opalescent - the sign that the anisotropic liquid crystalline state has been reached. For many polymers which are polydisperse in molecular weight, as the concentration is increased beyond the critical concentration, a two-phase region appears containing first anisotropic domains in an isotropic matrix, and as concentration is further increased, isotropic domains in an anisotropic matrix, and finally completely anisotropic material. The viscosity is at a maximum in this biphasic region, and continually drops as the anisotropic component increases. Thus, it can be

seen that it is often advantageous to process LLCPs in the fully anisotropic state, where the viscosity is at a minimum.

What causes a polymer to behave as a liquid crystalline material? The main reason is extremely rigid segments (mesogenic units or mesogens) which are either in the polymer backbone (main chain LCPs) or on the side chains with a flexible backbone (side chain LCPs). The chain of the liquid crystal may also consist of mesogenic units and flexible spacers as described in Figure 3.4. The flexible spacers are usually added to increase polymer solubility, but they almost always cause a degradation of the physical properties of the finished article (typically film or fiber).

As was mentioned previously, the anisotropic alignment of several polymer chains into a subunit is usually called a domain. It is possible to arrange several domains into liquid crystal supramolecular structures. There are two main supramolecular structures in liquid crystals: nematics and smectics. Figure 3.5 shows these two structures. The nematic polymer has a uniaxial alignment of approximately parallel domains with the segments randomly translated along the x-axis . The smectic polymer has segregated layers of domanial structures. Both nematic and smectic LLCPs will exhibit an ordered domanial microstucture at rest when they are beyond the critical concentration. In addition, a high degree of molecular orientation can be achieved with these materials when they are processed under certain conditions. This leads to finished articles (fibers and films) in which a directional variation of mechanical properties is observed. Thus, for these LLCPs the processing conditions are extremely important for the finished product mechanical properties. As might be expected, the rheological (flow) properties of these anisotropic and inhomogeneous solutions of rigid molecules is much more complex than the typical isotropic and flexible

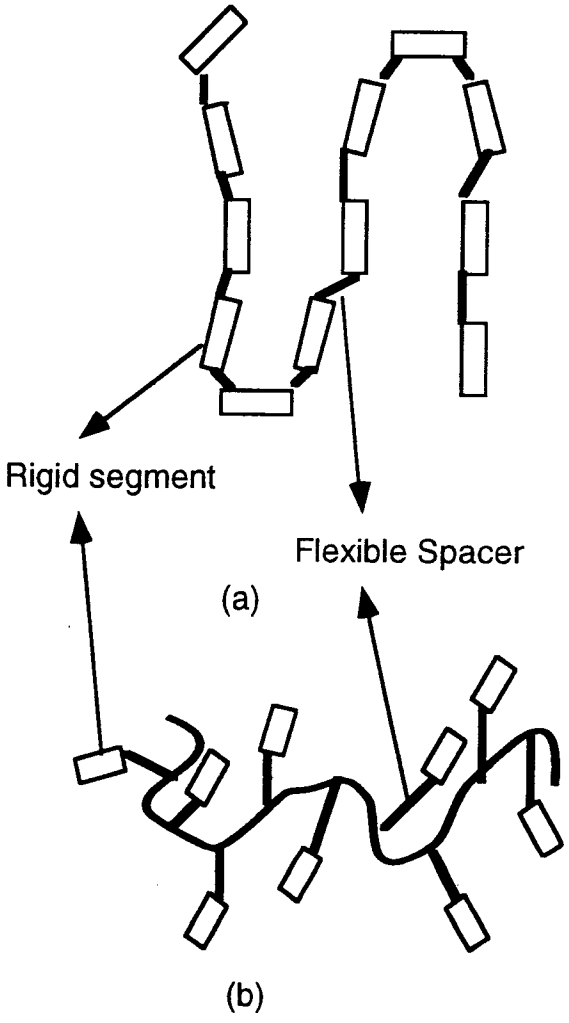

Figure 3.4 The structure of a polymer chain in the liquid crystalline state (a) rigid segments in the main chain (b) rigid segments in the side chains

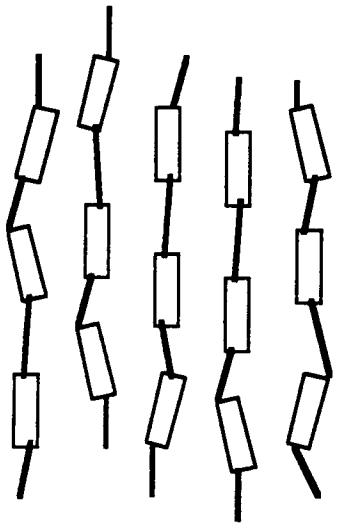

(a)

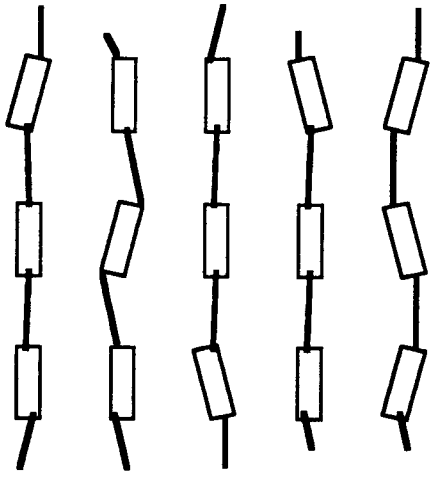

(b)

Figure 3.5 Liquid crystal structure (a) nematic (b) smectic

macromolecules in solution. Nematic, anisotropic solutions exhibit a number of anomalous flow behaviors attributed to their organized domanial structures. Of these, the most relevant to these studies are: lack of time-temperature superposition; extremely high zero-shear viscosity with a pronounced shear-thinning character attributed to the rearrangement and alignment of the domanial regions; reduced extrudate (die) swell in high shear extrusion due to alignment of the rigid domains. The significance of these behaviors to the modeling studies for the particular LLCP system of interest will be discussed in the next section.

3.5 Rheological characteristics of poly (*p*-phenylene-cis-benzobisoxazole) in Polyphosphoric Acid (PBO/PPA)

The modeling studies presented in this thesis were motivated by a need to design a film die for the production of high performance, thin films from the liquid crystal polymer poly (p-phenylene-cis-benzobisoxazole), a rigid backbone polymer whose repeat unit structure is given in Figure 3.6.

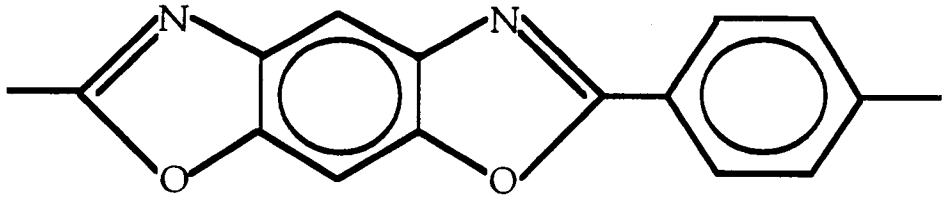

Figure 3.6 The repeat unit for poly (*p*-phenylene-cis-benzobisoxazole)

This polymer is of great technological interest because the mechanical properties of films and fibers fabricated from lyotropic solutions of this polymer in strong acid solvents, rank close to the highest ever achieved for organic materials. In addition, cis-PBO has superior thermal stability and chemical resistance. Because of it's stiff backbone cis-PBO is not soluble in ordinary organic solvents. It is usually synthesized, characterized, and processed in strong acids, such as polyphosphoric acid and methanesulfonic acid. The details of the polymerization techniques and solution characteristics of cis-PBO can be found in the works of Roitman and co-workers (1993a, 1993b).

The system of particular interest for the film die modeling studies was 14 wt% cis-PBO in polyphosphoric acid (PBO/PPA), the rheological (flow) characteristics of which were studied by Ernst and co-workers (1992) and James and co-workers (1995). In particular, the latter research group obtained capillary flow data for the PBO/PPA system over a wide range of flow temperatures (75 °C - 150°C) and shear rates. To summarize their results, they found that the 14 wt% PBO/PPA solutions followed power-law fluid behavior in the shear rate range of 1 - 1000 s^{-1}, and that there was substantial extrudate swell (50 - 80%) at low temperatures (75 - 100°C) and high shear rate, which rapidly fell off to almost no extrudate swell at 150°C up to shear rates of 300 - 500 s^{-1}. They also measured the density of 14 wt% PBO solution to be 2000 Kg / m^3.

The processing of PBO/PPA to make high performance film was carried out at The Dow Chemical Research Laboratories (Walnut Creek, CA), using an 8 inch (approx. 0.2m) coathanger film die with an "off-the-shelf" design. The film die was run at T = 150 - 180°C, and at these conditions the power-law model for the 14 wt% PBO/PPA solution was found to be:

$$\eta = K\dot{\gamma}^{n-1} \qquad K = 10000\ Pa \cdot \sec \qquad n = 0.12 \qquad \text{Equation 3.2}$$

As one can see from Equation 3.2, the PBO/PPA solution is a very shear thinning material. Viscosity data were almost the same in the temperature regime from 150 $^{\circ}C$ to 180 $^{\circ}C$, indicating that the 14 wt% PBO/PPA solution appeared to be in the "fully nematic" liguid crystalline regime at T=180°C. The first step in the PBO film manufacturing process used at Dow was the extrusion of the PBO/PPA through an 8 inch (approx. 0.2 m) wide laboratory film die

In this film extrusion, there was always a problem with internal structure in the film (domains causing opaque bands to form) and uneven flow distribution across the die width. This provided the motivation for this study, which was to design a film die for this process which would give uniform flow rate at the die exit, and hopefully eliminate the central band region.

In general, it would be useful to use a viscoelastic constitutive equation for the PBO/PPA solutions. However, as mentioned earlier, the capillary flow experiments of James and co-workers (1995) indicate that at typical film extrusion conditions (i. e., relatively low shear rate and T=150 - 180 $^{\circ}C$), the extrusion swell(elasticity) was minimal. Coupled with the special precautions taken in die design to eliminate sharp corners and contractions in the manifold and prelanding zone, it should be the viscous, and not viscoelastic, forces which dominate. Thus the power-law model, which is purely viscous, should suffice for the modeling studies.

3.6 Geometry and dimensions of the laboratory coathanger die

As can be seen in Figure 3.7, the linearly tapered coathanger die has gentle transitions in geometry which should lend itself to smooth flow patterns. In addition, a manifold having a teardrop cross-sectional shape was chosen, which has a smoother flow pattern than a manifold having a circular cross-section. This is the current trend in film die design. The main features of the coathanger die, as depicted in Figure 3.7, are the linearly tapered manifold section with a teardrop shape, the prelanding zone, and the landing zone extending to the die exit. In many die designs there are additional features (see Figure 2.1) such as a choker bar in the landing zone region, to allow for changes in channel height(H_2), and adjustable die lips, to allow for variable height across the width at the die exit. These are both "accessories" that allow for fine tuning of the die to maintain uniform film thickness at the die exit. Since the purpose of these studies was to find the optimal die geometry it wasn't necessary to include these options in the parametric study for the optimized manifold and die design.

The approximate dimensions of the die were chosen to match those of a laboratory scale film die used by The Dow Chemical Company (Walnut Creek, CA) for the production of thin, high performance films from the lyotropic LCP system of PBO/PPA solutions. With reference to Figure 3.7 once again, the die width W was 0.2 m ; the initial radius R_o of the manifold was 0.005 m ; the height of the prelanding zone H_1 was 0.002 m ; the height of the landing zone H_2 was 0.001 m and the teardrop cross-section angle was 60 °. The inlet channel was of circular cross-section (R = 0.005 m) with a length of 0.06 m, which was shown through the computer simulations to be of

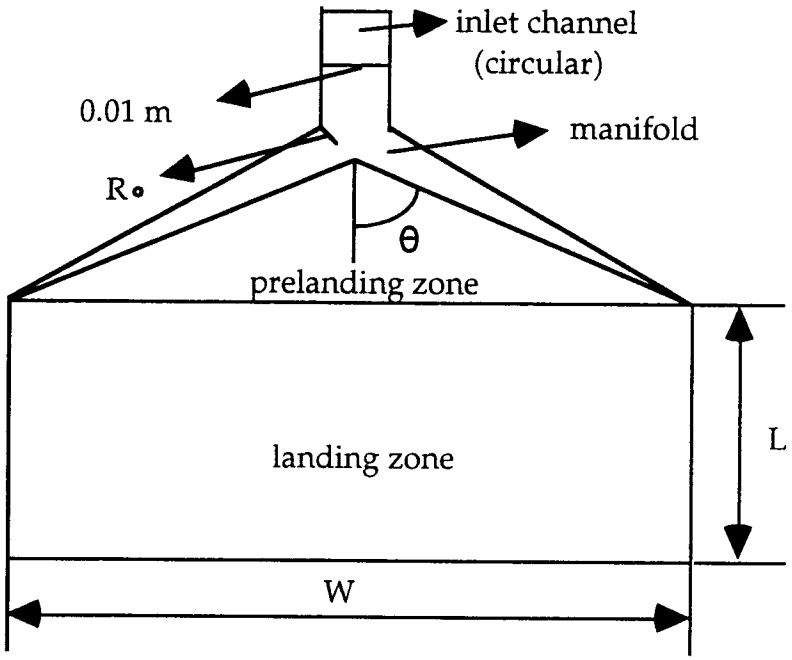

(a)

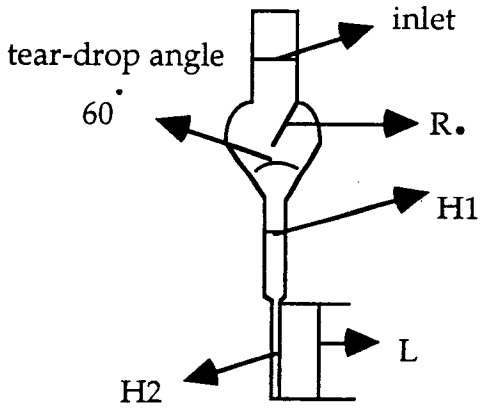

(b)

Figure 3.7 Coathanger Die (a) plan view (b) side view

sufficient length to get a fully developed velocity profile into the manifold section even for values of n = 0.12 (see the inlet channel in Figure 3.8).

The equation derived by Chung and Lohkamp (1976) was used to choose the variables for the parametric study of film die geometry. The derivation of Equation 3.3 is summarized in Appedix 3.

$$R_o = \left[\frac{(3n+1)}{4\pi(2n+1)} W\right]^{\frac{n}{(3n+1)}} \left[\frac{H_1^{\frac{(2n+1)}{(3n+1)}}}{\cos\theta^{\frac{1}{(3n+1)}}}\right] \qquad \text{Equation 3.3}$$

This simplified equation was derived using the following assumptions:

(1) Polymer melt or solution viscosity can be described by the power-law equation.

(2) The temperature of the fluid is uniform throughout the flow stream (isothermal system).

(3) The geometry of the coathanger die is ideally designed, so that the flow rate from the manifold into the prelanding zone is the same over the entire length of the manifold, and polymer melt in the prelanding zone flows only along the machine direction.

(4) There are only two independent flow components, one component along the manifold, and the other into the prelanding zone.

(5) The die has a circular type manifold and the heights of the prelanding and landing zones are constant.

As can be seen from the Equation 3.3, the manifold angle θ is dependent upon the die width W, the initial radius R_o, the power-law index n , and the height of the prelanding zone H_1. Therefore, once the die width, W is fixed by market or production considerations, other variables such as R_o, H_1 and θ must be chosen. For the parametric study, R_o and H_1 were already

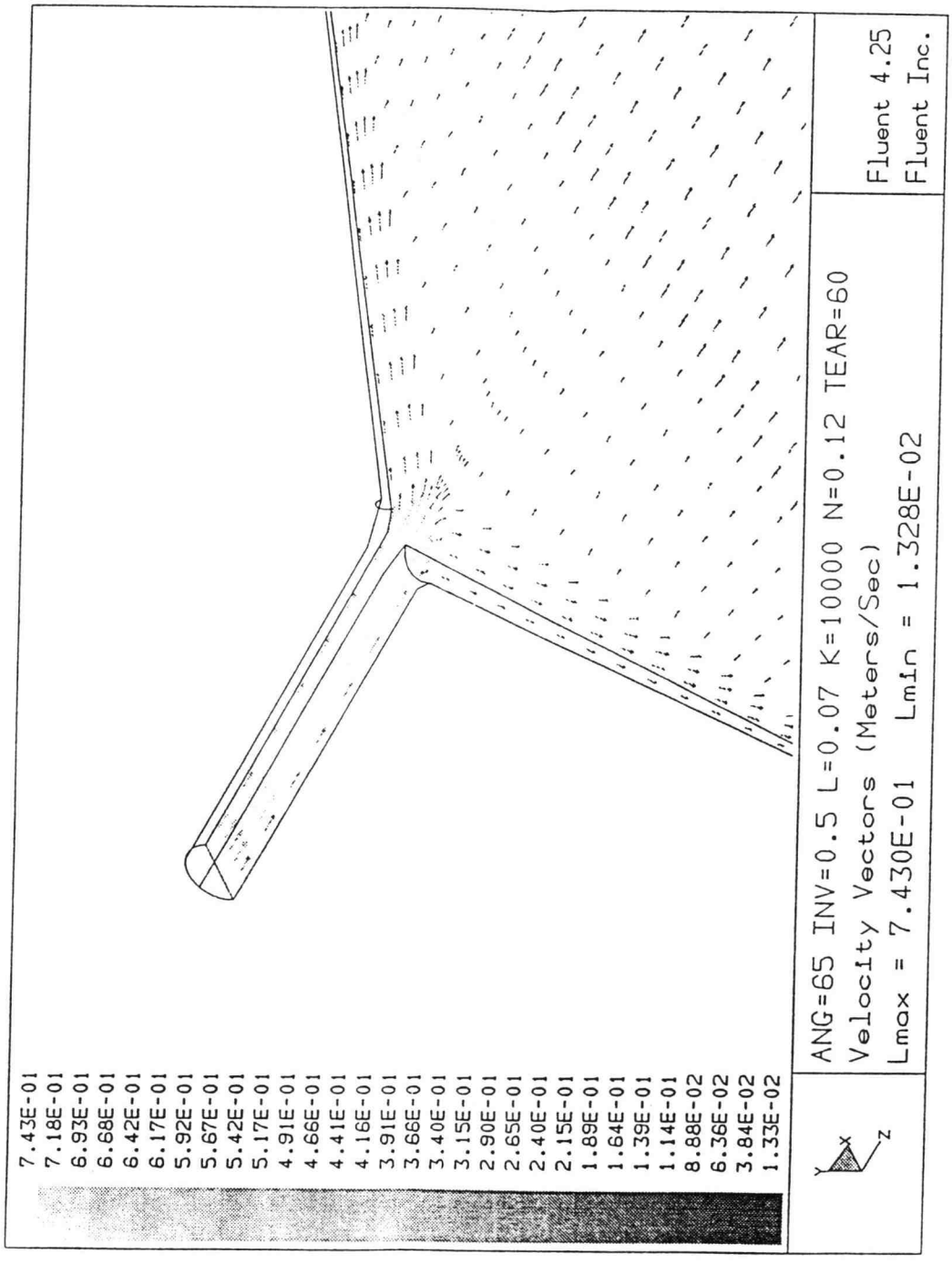

Figure 3.8 Vector velocity plot near inlet channel region on the symmetry surface of the coathanger die for inlet velocity $w = 0.5\,m/\sec$, length of landing zone $L = 0.07\ m$, $K = 10000\ Pa\cdot\sec$, manifold angle $\theta = 65^{\circ}$, power-law index $n = 0.12$

set, therefore the three main independent variables chosen were the manifold angle θ, the inlet velocity (or flow rate), and the length of the landing zone L.

Since FLUENT performs the full 3-D calculations, it is not necessary to use all the assumptions that Chung and Lohkhamp (1976) used in their derivation of the Equation 3.3. *In the present simulation, only two assumptions were made: that the fluid is isothermal and that it behaves as a power-law fluid.*

A comment on the two assumptions is appropriate at this point. The isothermal fluid assumption is probably a good one. Generally, in the laboratory these films are produced at moderately slow rates (approximately 1 linear foot per minute), such that it would be expected that the solution in the die would be fairly close to the temperature at the die wall and uniform both across the width and along the length. The slow rates preclude any substantial temperature variations due to viscous heating.

The assumption of a power-law fluid is somewhat more tenuous. There is a substantial body of literature which states that LCP's exhibit very little viscoelastic characteristics, as determined by little or no extrudate swell in capillary viscosity measurements. However, some recent data by James, Denn, Pierini, and Rochefort (1995) on the PBO/PPA system which is of interest in these studies, shows that up to 50% extrudate swell is observed in capillary viscosity measurements. This might raise some concern about the validity of the purely viscous power-law model for the PBO/PPA system. However, the data of James, Denn, Pierini, and Rochefort (1995) also show that extrudate swell decreased dramatically at higher temperatures and lower shear rates. In fact, their data indicate that at 180 $^{\circ}C$ and a shear rate of 10 - 500 sec^{-1} there is virtually no extrudate swell. The maximum shear rate in the

coathanger die simulations was approximately 30 sec^{-1} for the die width W = 0.2 m, the manifold angle $\theta = 85^{\circ}$, the height of the landing zone $H_2 = 0.001$ m, the height fo the prelanding zone $H_1 = 0.002$ m,and the inlet velocity w = $0.5 m / \sec$. Thus, for the particular operating conditions being used in this study for the PBO/PPA system, the power-law model should be a very reasonable approximation.

The following scenario was followed for the die geometry parametric study. First, the simulations were performed with $\theta = 82^{\circ}$ (calculated from the Equation 3.3 with $W = 0.2$ m, $R_o = 0.005$ m, $H_1 = 0.002$ m, and $n = 0.12$), and $L = 0.05$ m with various inlet velocities. After the above simulations, the manifold angle θ was changed at constant inlet velocity and length of the landing zone L to obtain the optimal manifold angle θ. After obtaining the optimal manifold angle, for the given condition, the length of the landing zone L was varied to determine the asymptotic region related to fully developed flow. To examine the effects of fluid properties, the simulations were performed with various K values and several power-law indices (n) at constant manifold angle θ, inlet velocity, and length of the landing zone L. The following is a detailed list of the various case studies that were performed with the coathanger die geometry.

(1) Flow rate distributions with different inlet velocities, w

Constant

manifold angle $\theta = 82^{\circ}$

14 wt% PBO/PPA solution density = 2000 Kg / m^3

length of landing zone $L = 0.05$ m

$K = 10000$ $Pa \cdot \sec$

power-law index $n = 0.12$

Variable

inlet velocity, $w = 0.1\,m/\sec, 0.2\,m/\sec, 0.4\,m/\sec, 0.6\,m/\sec$, and $0.8\,m/\sec$

(2) Flow rate distributions with different inlet manifold angles

Constant

14 wt% PBO/PPA solution density = 2000 Kg/m^3

length of landing zone $L = 0.05\ m$

$K = 10000\ Pa \cdot \sec$

power-law index $n = 0.12$

inlet velocity, $w = 0.5\,m/\sec$

Variable

manifold angle $\theta = 55^\circ, 63^\circ, 65^\circ, 66^\circ, 75^\circ, 82^\circ$, and 85°

(3) Flow rate distributions with different lengths of landing zone

Constant

14 wt% PBO/PPA solution density = 2000 Kg/m^3

$K = 10000\ Pa \cdot \sec$

power-law index $n = 0.12$

inlet velocity, $w = 0.5\,m/\sec$

manifold angle $\theta = 65^\circ$

Variable

length of landing zone $L = 0.001\ m, 0.01\ m, 0.03\ m, 0.05\ m$, and $0.07\ m$

(4) Flow rate distributions with different K-values for various manifold angles

Constant

14 wt% PBO/PPA solution density = 2000 Kg/m^3

power-law index $n = 0.12$

inlet velocity, $w = 0.5\,m/\sec$

length of landing zone $L = 0.05\ m$

Variable

manifold angle $\theta = 55^\circ, 65^\circ$, and 85°

$K = 1000\ Pa \cdot \sec, 5000\ Pa \cdot \sec$, and $10000\ Pa \cdot \sec$

(5) Flow rate distributions with different n-values for various manifold angles

Constant

14 wt% PBO/PPA solution density = $2000\ Kg / m^3$

inlet velocity, $w = 0.5 m / \sec$

length of landing zone $L = 0.05\ m$

$K = 10000\ Pa \cdot \sec$

Variable

manifold angle $\theta = 55^\circ, 65^\circ$, and 85°

power-law index n = 1.0 (Newtonian fluid), 0.8, 0.6, 0.4, 0.2, and 0.12

CHAPTER 4 : RESULTS AND DISCUSSION

A 40x6x30 grid with 7200 grid points was set-up for the coathanger die shown in Figure 4.1. For the 3-D geometry, calculations were performed at each node point. There are 39 (= 40 - 1) calculation points (nodes) in x-axis direction, 5 (= 6 - 1) nodes in y-axis direction, and 29 (= 30 - 1) nodes in z-axis direction. At the outlet surface of the die, there are 195 (39 x 5) nodes. Therefore, there are 6 values of mass flow rate at each x-axis position including the boundary condition at the wall. At the wall, the fluid velocities all have zero values due to the no-slip condition (total x-axis position = 41 at outlet including the boundary condition at wall). To determine the flow rate distributions, the average flow rate at each x-axis position was calculated by adding the six values (5 values at nodes and zero at wall) and then dividing by six. The zero value at wall was added to include the steep gradient of flow rates and shear rates near the wall region for the calculation of the average flow rate.

4.1 Flow rate distributions at the die exit with different inlet flow rates

The simulation was performed with the manifold angle $\theta = 82\ ^{\circ}$ and the length of the landing zone $L = 0.05\ m$ when the inlet flow rates are $7.8540 \times 10^{-6}\ m^3/\sec$ ($w = 0.1\,m/\sec$), $1.5708 \times 10^{-5}\ m^3/\sec$ ($w = 0.2\,m/\sec$), $3.14159 \times 10^{-5}\ m^3/\sec$ ($w = 0.4\,m/\sec$), $4.71239 \times 10^{-5}\ m^3/\sec$ ($w = 0.6\,m/\sec$), and $6.28319 \times 10^{-5}\ m^3/\sec$ ($w = 0.8\,m/\sec$). Where w is the average inlet velocity.

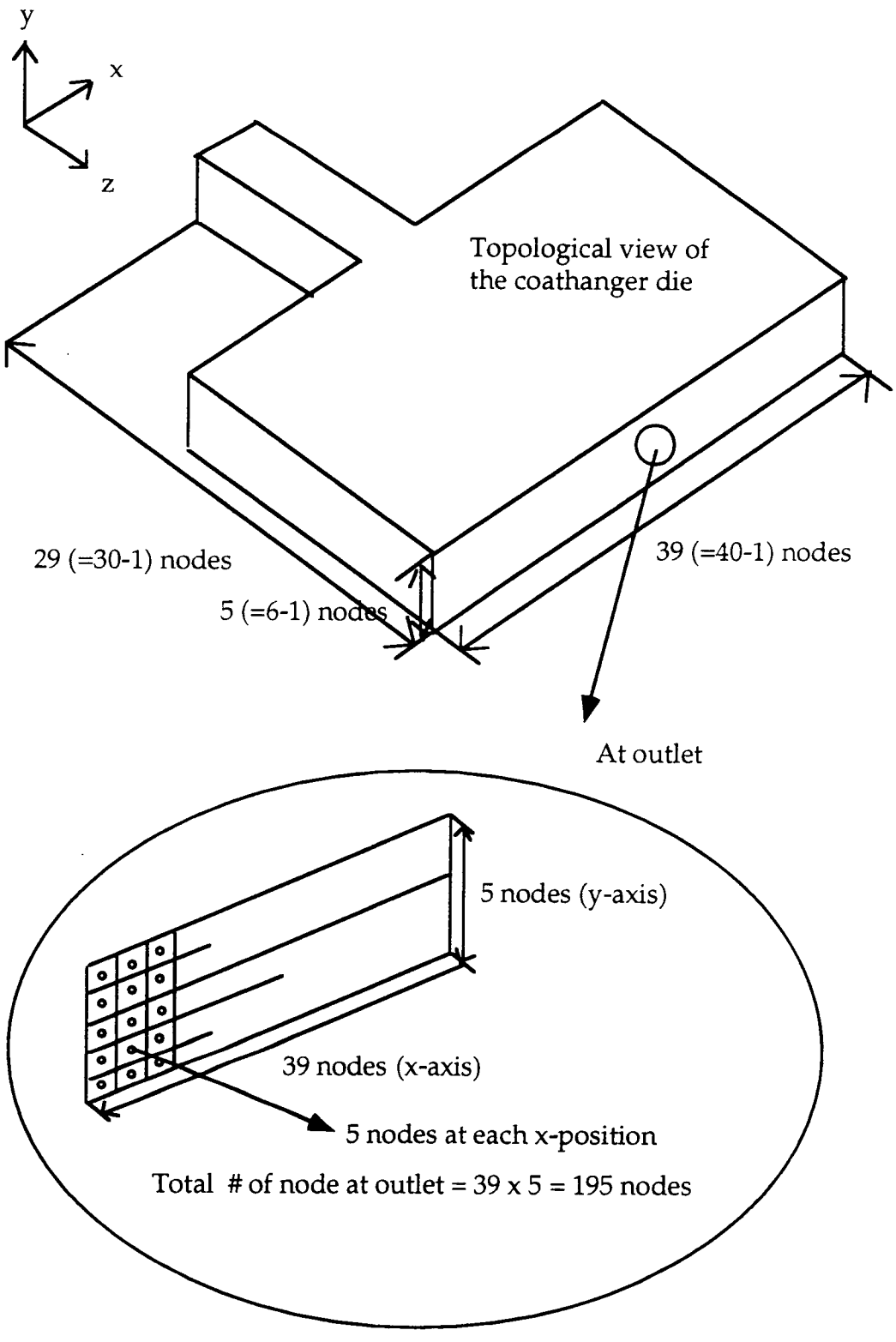

Figure 4.1 Set-up of grid for the coathanger die on curvilinear body-fitted coordinates (BFC)

The inlet flow rate can be calculated by multiplication of the cross-sectional area of the inlet ($7.85398 \times 10^{-5} m^2 / \sec$) with the average inlet velocity . The power-law data for the PBO/PPA solution ($\eta = K\dot{\gamma}^{n-1}$, $K = 10000\ Pa \cdot \sec$, and $n = 0.12$) was used for the simulation. As you can see in Figure 4.2 and Figure 4.3, there is no value of the inlet flow rate at which the die has a relatively uniform film thickness distribution across the width (x-direction). As the inlet flow rate (or the average inlet velocity) is increased, the difference between the maximum value of the flow rate near the center region and the minimum at the wall region increases. Hence, the inlet flow rate is not a critical independent parameter to optimize the performance of the coathanger die. For this reason, an arbitrary intermediate value of inlet flow rate, 3.9270 $m^3 / \sec (w = 0.5 m / \sec)$ was chosen for the remaining simulations in the parametric study.

4.2 Flow rate distributions at the die exit with different manifold angles

The simulation was performed with the length of the landing zone $L = 0.05\ m$,the inlet flow rate = 3.9270 $m^3 / \sec (w = 0.5 m / \sec)$, and the manifold angle $\theta = 85^\circ, 82^\circ, 75^\circ, 66^\circ, 65^\circ, 63^\circ$, and 55°. The power-law data for the PBO/PPA solution ($\eta = K\dot{\gamma}^{n-1}$, $K = 10000\ Pa \cdot \sec$, and $n = 0.12$) is the same as in the previous section. As you can see in Figures 4.4, 4.5 and 4.6, there is a value of the manifold angle θ at which the fraction of die width at the exit with uniform flow rate (film thickness) is maximized. As the manifold angle θ is decreased from 85° to 65° the region having a uniform flow rate broadens. Decreasing the manifold angle θ from 65° to 55°, the region of

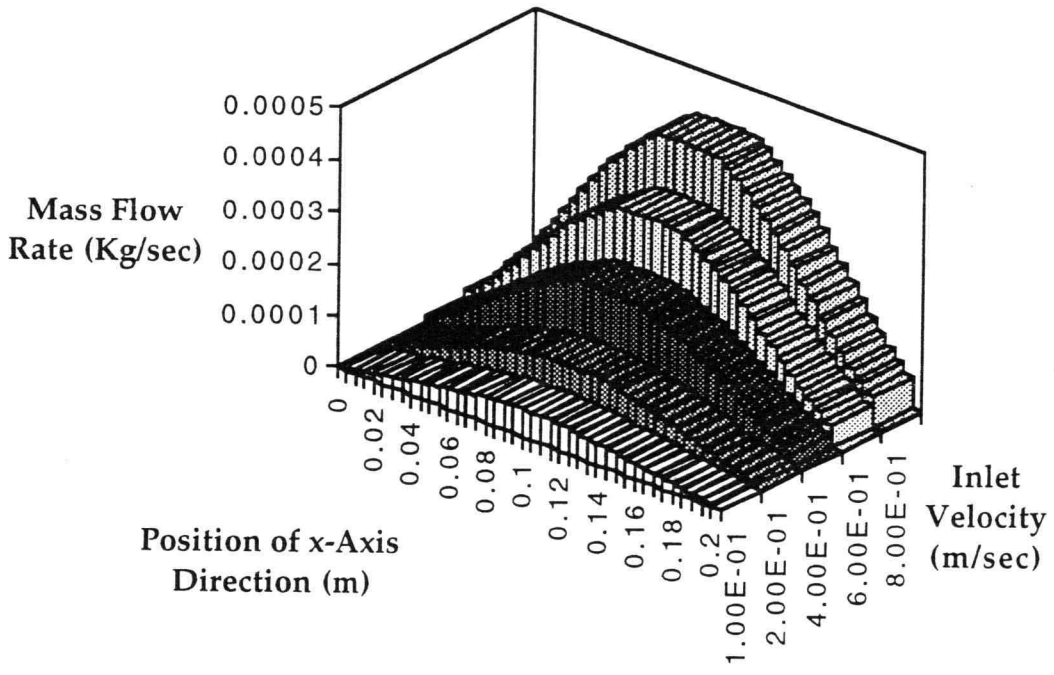

Figure 4.2 Flow rate distributions at the die exit for various inlet velocities.
Power-Law Fluid ($K = 10000\ Pa \cdot \sec$; $n = 0.12$),
Length of Landing Zone $L = 0.05\ m$,
Manifold Angle $\theta = 82^\circ$

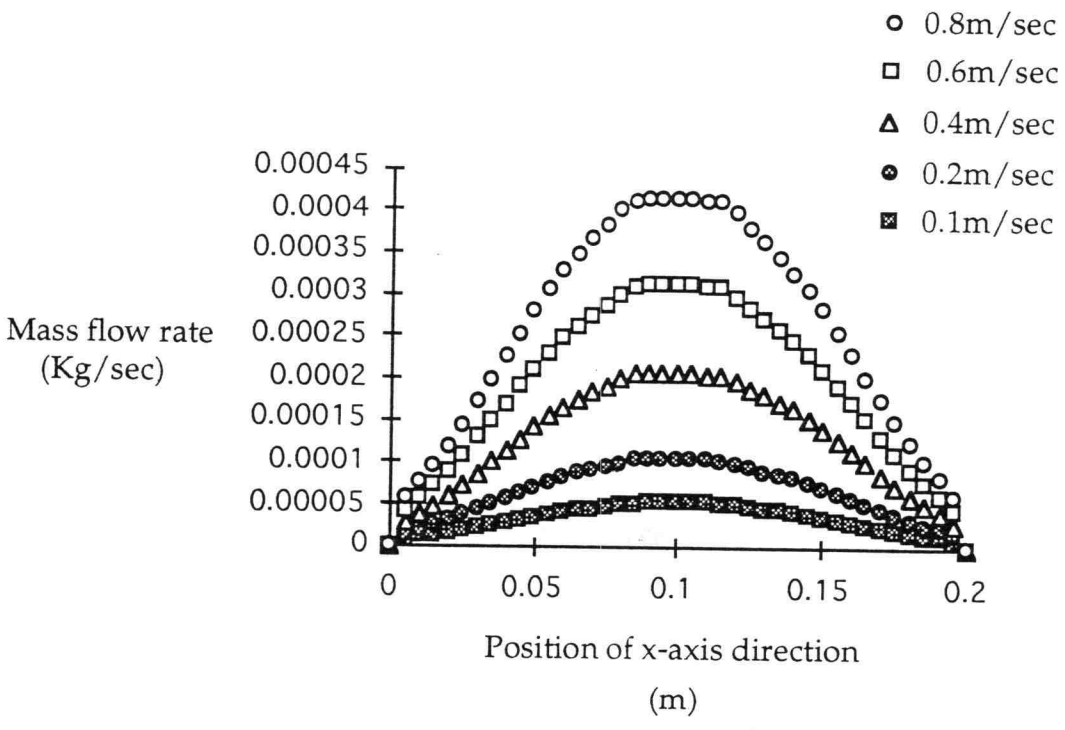

Figure 4.3 Flow rate distributions at the die exit for various inlet velocities.
Power-Law Fluid ($K = 10000\ Pa \cdot \sec$; $n = 0.12$),
Length of Landing Zone $L = 0.05\ m$,
Manifold Angle $\theta = 82^{\circ}$

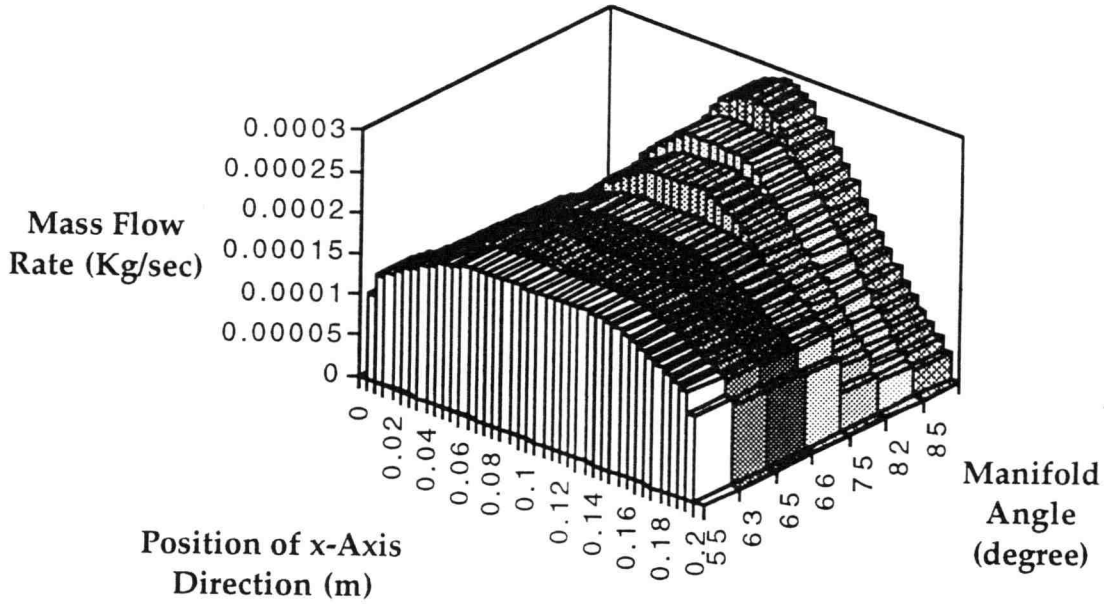

Figure 4.4 Flow rate distributions at the die exit for various manifold angles.
Power-Law Fluid (K = 10000 $Pa \cdot \sec$; n = 0.12),
Length of Landing Zone L = 0.05 m,
Inlet Velocity = 0.5 $m / \sec$

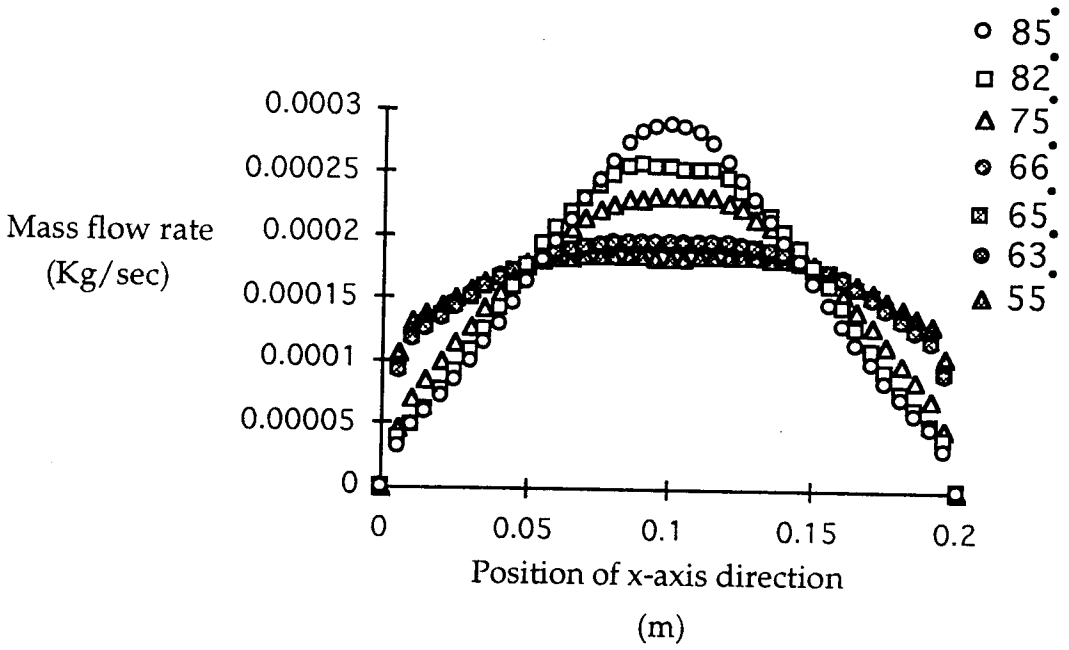

Figure 4.5 Flow rate distributions at the die exit for various manifold angles.
Power-Law Fluid (K = 10000 $Pa \cdot \sec$; n = 0.12),
Length of Landing Zone L = 0.05 m,
Inlet Velocity = 0.5 $m / \sec$

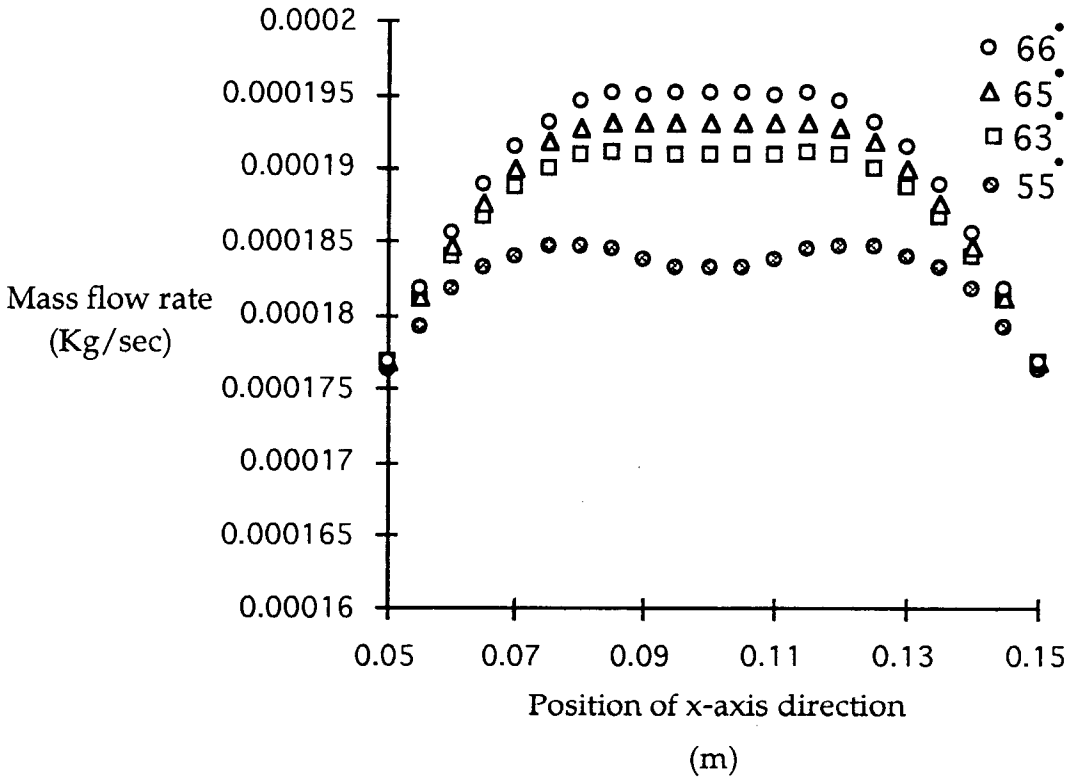

Figure 4.6 Flow rate distributions at the die exit for various manifold angles.
Power-Law Fluid (K = 10000 $Pa \cdot \sec$; n = 0.12),
Length of Landing Zone L = 0.05 m,
Inlet Velocity = 0.5 m / sec

uniform flow rate shrinks and finally a drop in the flow rate appears at the center, disrupting the uniformity (Figure 4.6).

As could have been qualitatively predicted from the Equation 3.3, for the PBO/PPA system there is a preferred manifold angle which gives the broadest uniform film thickness at the die exit. However, the preferred angle predicted using the Equation 3.3 is 82°, while the computer simulation predicts $\theta = 65^{\circ}$ to give the most uniform film. This difference is most probably the result of three important assumptions made by Chung and Lohkamp (1976) in deriving Equation 3.3, but not necessary in the 3-D simulation. As outlined in section 3.6, the key assumptions were:

(1) The manifold has a circular cross-section

- the die geometry used in this study has a tear-drop cross-section.

(2) There are only two independent flow components, one component along the manifold, and the other into the prelanding zone.

- the present simulation is three dimensional, which allows for three independent flow components, both in the manifold and into the preland region.

(3) The geometry of the coathanger die are ideally designed, such the flow rate from the manifold into the prelanding zone is the same over the entire length of the manifold, and polymer melt in the prelanding zone flows only along the machine direction.

This is probably the most limiting assumption, particularly when trying to find an optimized coathanger die geometry, because flow in the most complicated flow region - the manifold to preland transition zone - is pre-specified to be uniform. One of the primary goals of this study, and any die design study for that matter, is to design the manifold to obtain uniform flow along the entire length of the manifold. In making that assumption Chung

and Lohkamp (1976) have effectively removed the manifold angle optimization problem from their analysis. The determination of a preferred manifold geometry with none of the above limiting assumptions was one of the major contribution of the 3-D simulation performed in this study.

As can be seen in Figure 4.5 and in an expanded x-y scale in Figure 4.6, the preferred manifold angle determined from the simulations is approximately $\theta = 63 - 65^\circ$ with $\theta = 65^\circ$ giving the largest uniform flow region across the die exit width. In Figure 4.7, the complete flow rate distribution as a function of height at the die exit is depicted for $\theta = 65^\circ$.

4.3 Flow rate distributions at the die exit with different lengths of landing zone

The effect of the landing zone length on the flow rate distribution at the die exit was examined for the manifold angle $\theta = 65^\circ$, the inlet flow rate = $3.9270\ m^3/\sec (w = 0.5\,m/\sec)$, a power-law fluid with $K = 10000\ Pa \cdot \sec$, and $n = 0.12$, and the following lengths of landing zone; $L = 0.001\ m, 0.01\ m, 0.03\,m, 0.05\ m$, and $0.07\ m$. Figures 4.8 and 4.9 show the flow rate distribution at the die exit as a function of the length of landing zone. For these simulations the manifold angle is set at the preferred value of $\theta = 65^\circ$ and the inlet velocity at $0.5\,m/\sec$. Under these conditions, it can be seen that the die exit flow rate distribution becomes more uniform with increasing length of the landing zone, but appears to be asymptotically approaching a point of minimal change at approximately $L = 0.05\ m$. It is obvious from Figure 4.9, that a minimum L is needed to have something approaching a uniform die exit flow rate distribution. That is, for very small L $(0.03\,m)$ an inflection appears at the center in the flow rate distribution with "humps" at either edge that grow in

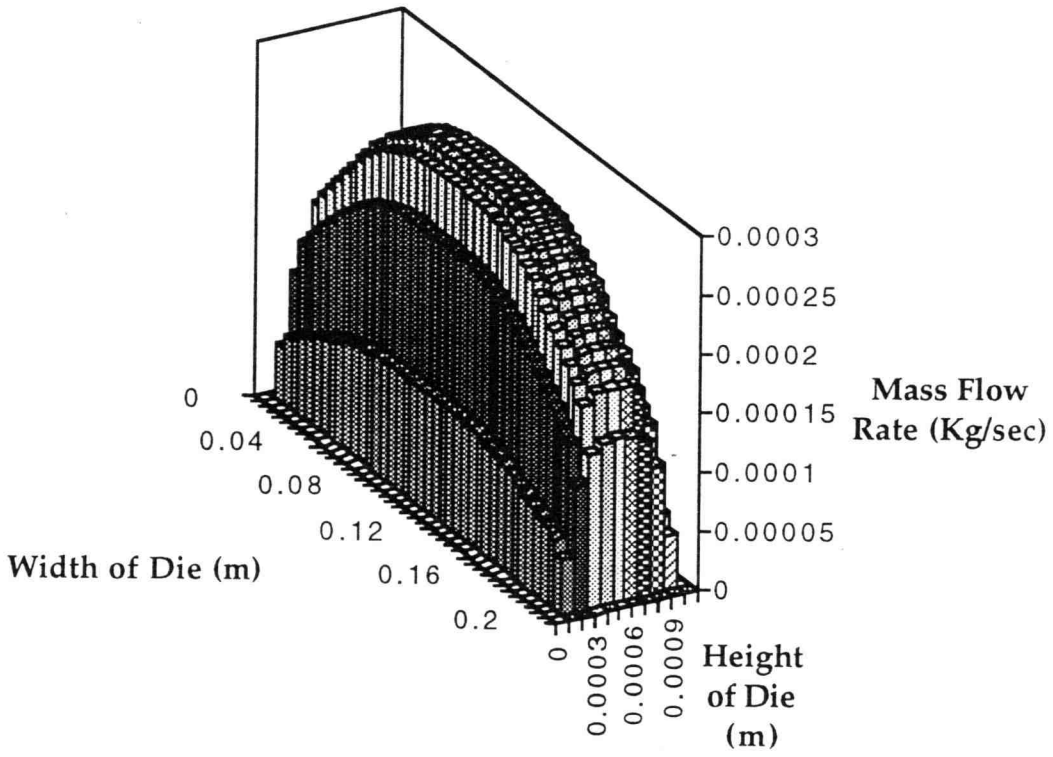

Figure 4.7 Flow rate distribution at the die exit for $\theta = 65^{\circ}$.
Power-Law Fluid ($K = 10000\ Pa \cdot \sec$; $n = 0.12$),
Length of Landing Zone $L = 0.05\ m$,
Inlet Velocity = 0.5 m / sec

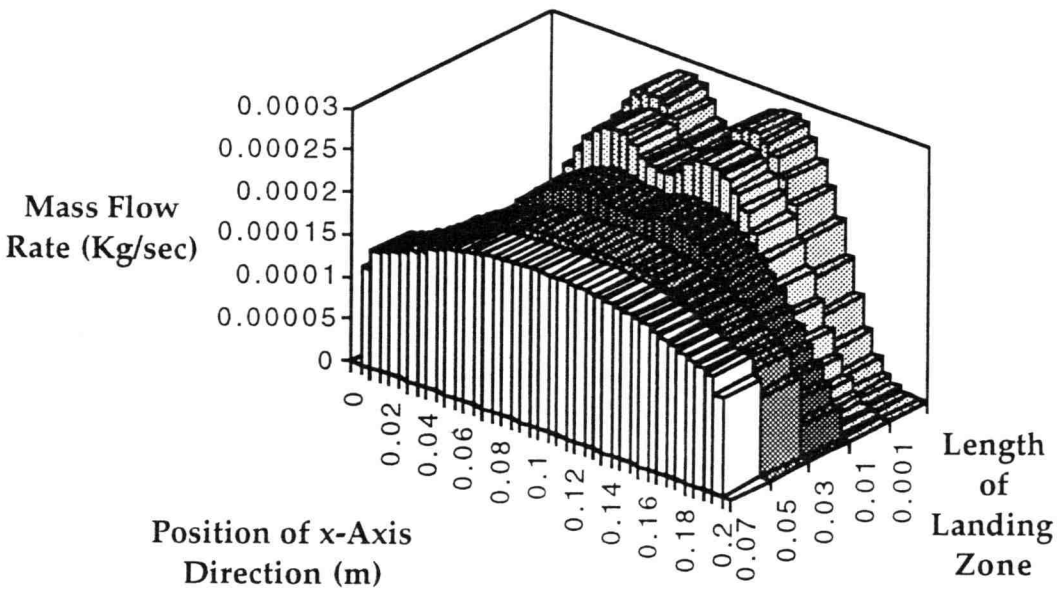

Figure 4.8 Flow rate distributions at the die exit for various lengths of landing zone. Power-Law Fluid (K = 10000 $Pa \cdot \sec$; n = 0.12), Inlet Velocity = 0.5 $m / \sec$, Manifold Angle $\theta = 65^{\circ}$

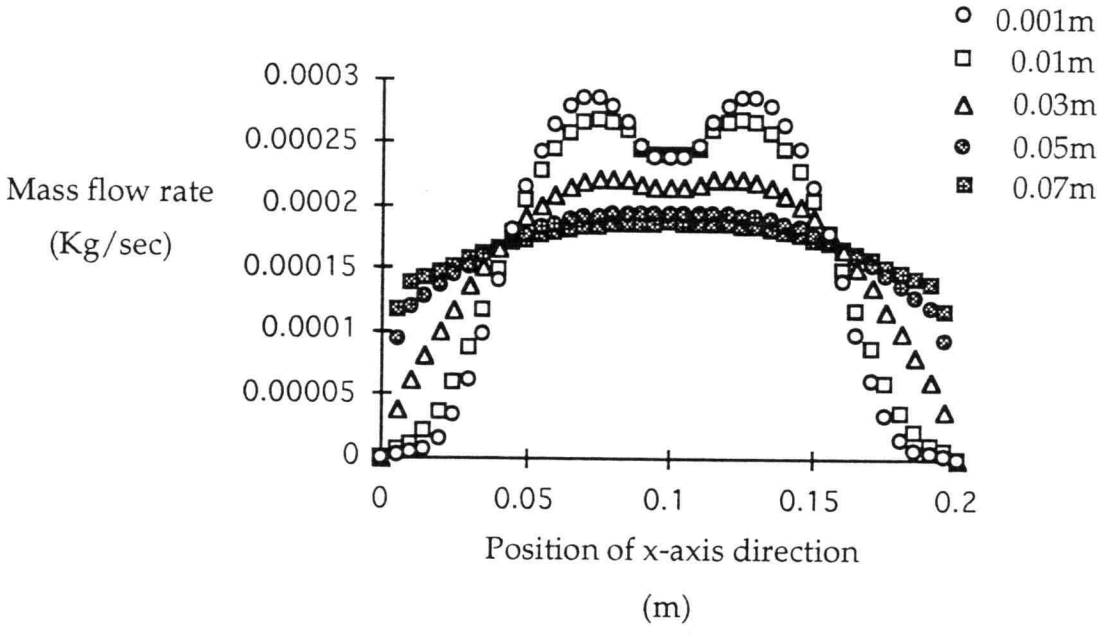

Figure 4.9 Flow rate distributions at die exit for various lengths of landing zone. Power-Law Fluid (K = 10000 $Pa \cdot \sec$; n = 0.12), Inlet Velocity = 0.5 $m/\sec$, Manifold Angle θ = 65°

size with decreasing L. Examining Equation 3.3, it would be predicted that the manifold angle is unaffected by the landing zone length. To look at that statement another way, the general behavior depicted in Figure 4.9 would be the same irrespective of the manifold angle chosen. This result is consistent with what one might expect from looking at the coathanger die geometry and the expected flow from the manifold region. Referring to Figure 3.7, the preland length is determined by the manifold angle θ, but for any θ chosen the farther down the manifold length the fluid travels, the shorter the distance it must travel in the machine direction to reach the die exit. Therefore, for very short landing zone lengths, one would expect a reduced mass flow rate in the center and a higher mass flow rate at either edge. This is exactly what is predicted in Figure 4.9 for landing zone length $L < 0.03\ m$. Using a similar argument, the preland length will not change dramatically with the manifold angle in the range $\theta = 55^\circ - 85^\circ$ (i.e., the preland length is not a strong function of θ). Therefore, the length of the landing zone to give a uniform mass flow rate distribution at the die exit should also not be a strong function of θ. Once the asymptotic value of the landing zone length mentioned above is determined, as it was shown to be $L = 0.05\ m$ in Figure 4.9, it would not be expected to change dramatically for another manifold angle. It would most probably be more sensitive to fluid parameters and in particular the power-law index n. For this reason, the simulation results in Figure 4.9 are for the lowest n value used, where the effects should be most prominent. In this way, one can be certain that the landing zone length determined will be the maximum required to process any non-Newtonian fluid through the coathanger die.

The results outlined in Figures 4.8 and 4.9 have some important implications for commercial die design. To determine the asymptotic region

for the length of the landing zone for a given manifold angle, one would have to do more simulations at $L = 0.07\ m$. However, the fact that there is very little change between $L = 0.05\ m$ and $L = 0.07\ m$, indicates that one is near the asymptotic region. In a commercial application, there is a high priority placed on designing dies with a short landing zone length because this situation leads to lower pressure drop through the die, and consequently higher throughput. Data similar to those in Figure 4.9 are critical for choosing a landing zone length which is neither too short (which is catastrophic due to the grossly uneven flow rate distribution) nor too long (which leads to high pressure drop and low throughput). Thus, an preferred value of the landing zone length can be determined for a given manifold angle, inlet velocity, and power-law fluid.

4.4 Flow rate distributions at the die exit with different K values

In the simulations discussed to this point, the material parameters in the power-law model were always maintained at $K = 10000\ Pa \cdot \sec$, and n = 0.12. To examine the sensitivity of the simulation to the magnitude of the viscosity, the K value was varied ($K = 1000, 5000,$ and $10000\ Pa \cdot \sec$) with various manifold angles ($\theta = 55^\circ, 65^\circ,$and 85°). As can be seen in Figures 4.10, 4.11, and 4.12, there is virtually no effect of varying K value on the flow rate distribution for any manifold angle. This result is consistent with the predictions of Equation 3.3, in which there is no predicted dependence of manifold angle on K.

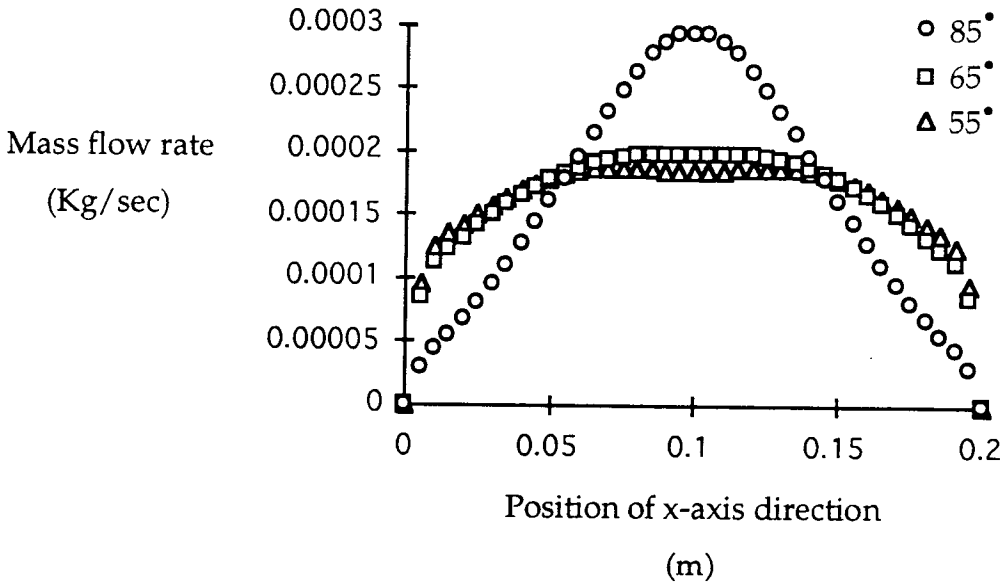

Figure 4.10 Flow rate distributions at the die exit for various manifold angles for $K = 1000\,Pa \cdot \sec$. Power-Law Index $n = 0.12$, Length of Landing Zone $L = 0.05\ m$, Inlet Velocity = 0.5 m / sec

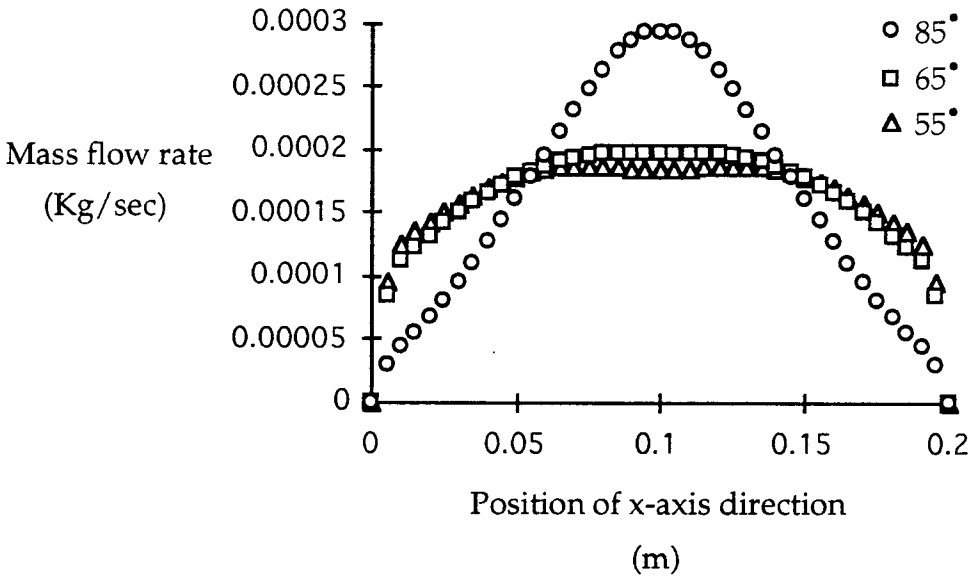

Figure 4.11 Flow rate distributions at the die exit for various manifold angles for $K = 5000\ Pa \cdot \sec$. Power-Law Index $n = 0.12$, Length of Landing Zone $L = 0.05\ m$, Inlet Velocity = 0.5 m / sec

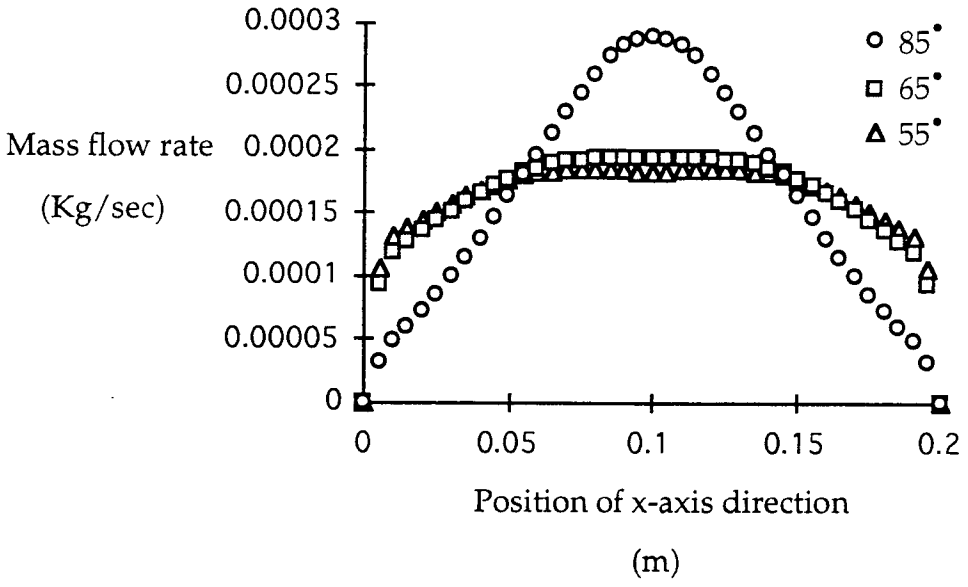

Figure 4.12 Flow rate distributions at the die exit for various manifold angles for $K = 10000\ Pa \cdot \sec$. Power-Law Index $n = 0.12$, Length of Landing Zone $L = 0.05\ m$, Inlet Velocity = 0.5 m / sec

4.5 Flow rate distributions at the die exit with different n values

The second important parameter in the power-law model is the power-law index (n), which determines the non-Newtonian nature of the fluid. As was indicated in earlier sections, lyotropic liquid crystal polymer solutions are, in general, extremely non-Newtonian with very low values of the power-law index. In order to examine the sensitivity of the simulation to the value of the power-law index used, various n values were tested (n = 1.0, 0.8, 0.6, 0.4, 0.2, and 0.12) with various manifold angles ($\theta = 55^\circ, 65^\circ$,and 85°). In fact, as was mentioned in section 3.3, in order to get faster convergence of the simulation, the n value was stepped down from n = 1.0 to n = 0.12 for all the simulations performed.

There are several interesting observations that can be made from the simulation data that are plotted in Figures 4.13 to 4.25. First, if one examines Figures 4.13 to 4.18 which are for n = 1.0, 0.8, and 0.6, respectively, it is clear that the n value has very little effect on the flow rate distribution at the exit, even for the largest manifold angle ($\theta = 85^\circ$). The implication is that for a fluid of moderate non-Newtonian character ($1.0 \geq n \geq 0.5$), there is essentially no preferred manifold angle; any manifold angle between $\theta = 55^\circ$ and $\theta = 85^\circ$ will give approximately uniform flow distribution at the die exit. However, for fluids that are highly non-Newtonian ($n < 0.5$), which includes many polymer melts and virtually all liquid crystal polymers (thermotropic or lyotropic), then the manifold angle chosen becomes important for obtaining a uniform flow rate distribution at the exit (Figures 4.19 to 4.22). For these highly non-Newtonian fluids, the concept of a preferred manifold angle is

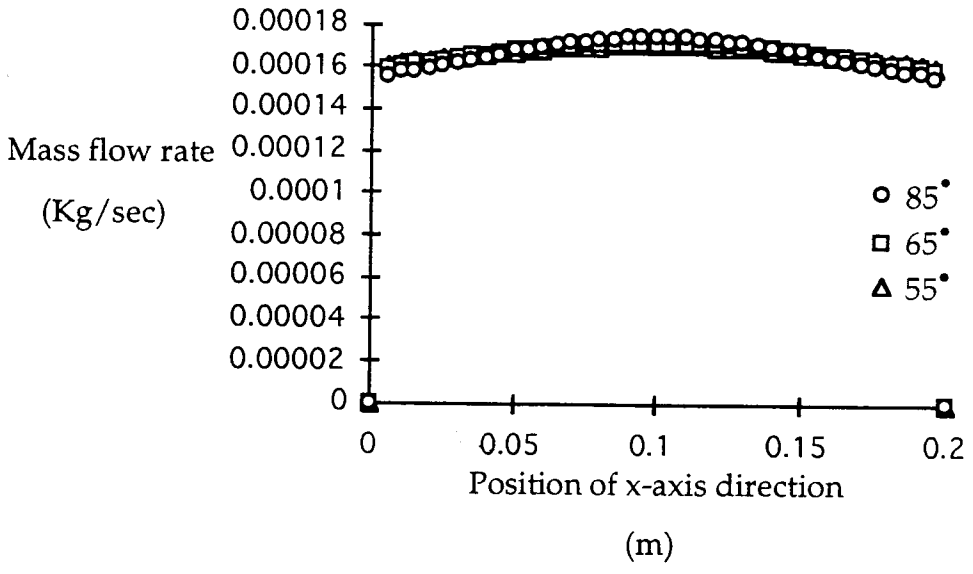

Figure 4.13 Flow rate distributions at the die exit for various manifold angles for n = 1.0 (Newtonian fluid).
K = 10000 $Pa \cdot \sec$,
Length of Landing Zone L = 0.05 m,
Inlet Velocity = 0.5 m / sec

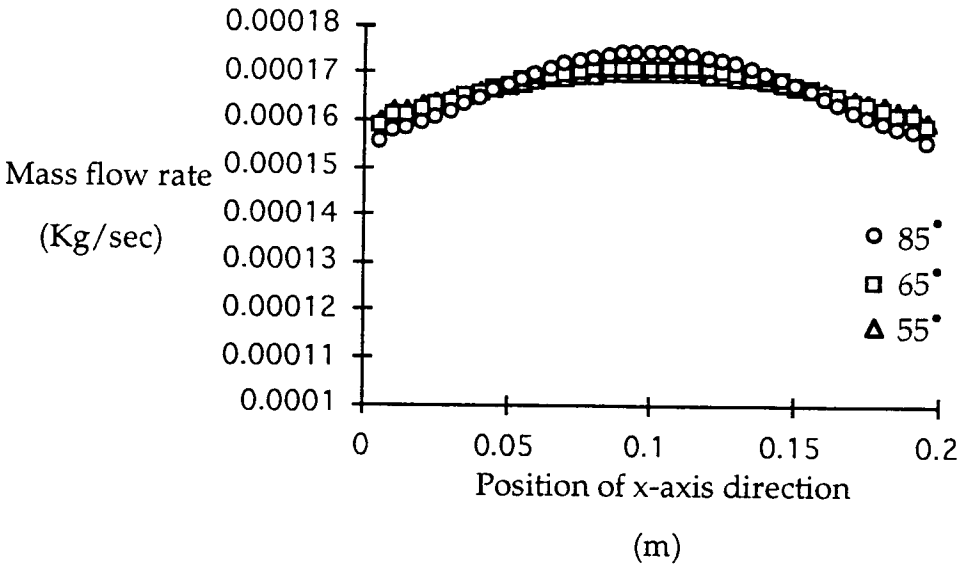

Figure 4.14 Flow rate distributions at the die exit for various manifold angles for n = 1.0 (Newtonian fluid).
K = 10000 $Pa \cdot \sec$,
Length of Landing Zone L = 0.05 m,
Inlet Velocity = 0.5 $m / \sec$

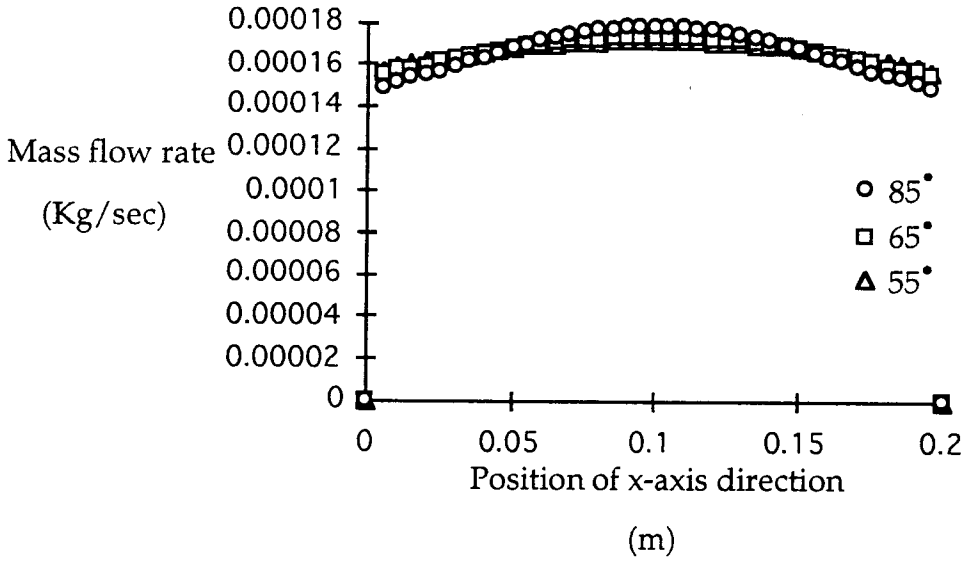

Figure 4.15 Flow rate distributions at the die exit for various manifold angles for $n = 0.8$.
$K = 10000\ Pa \cdot \sec$,
Length of Landing Zone $L = 0.05\ m$,
Inlet Velocity = 0.5 m / sec

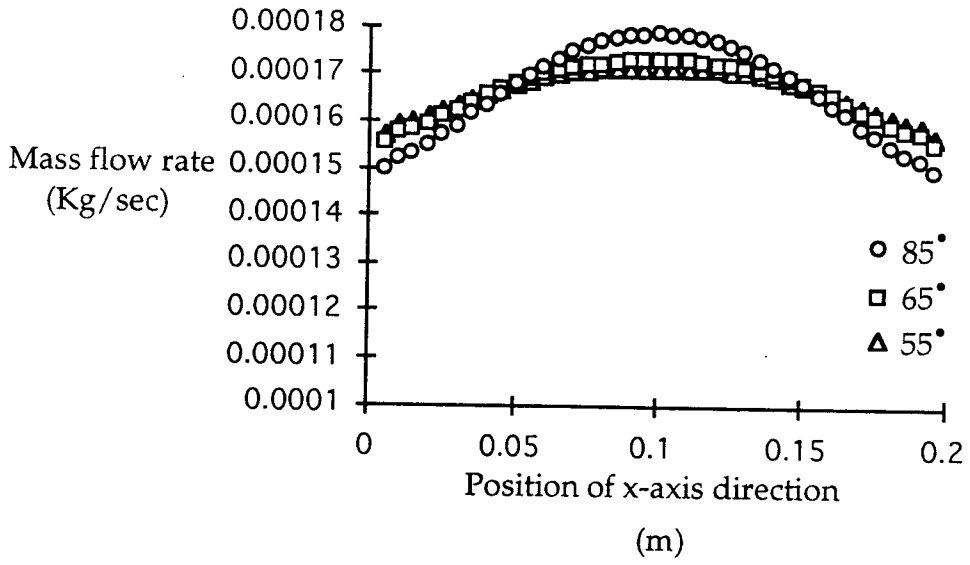

Figure 4.16 Flow rate distributions at the die exit for various manifold angles for $n = 0.8$.
$K = 10000\ Pa \cdot \sec$,
Length of Landing Zone $L = 0.05\ m$,
Inlet Velocity = 0.5 m / sec

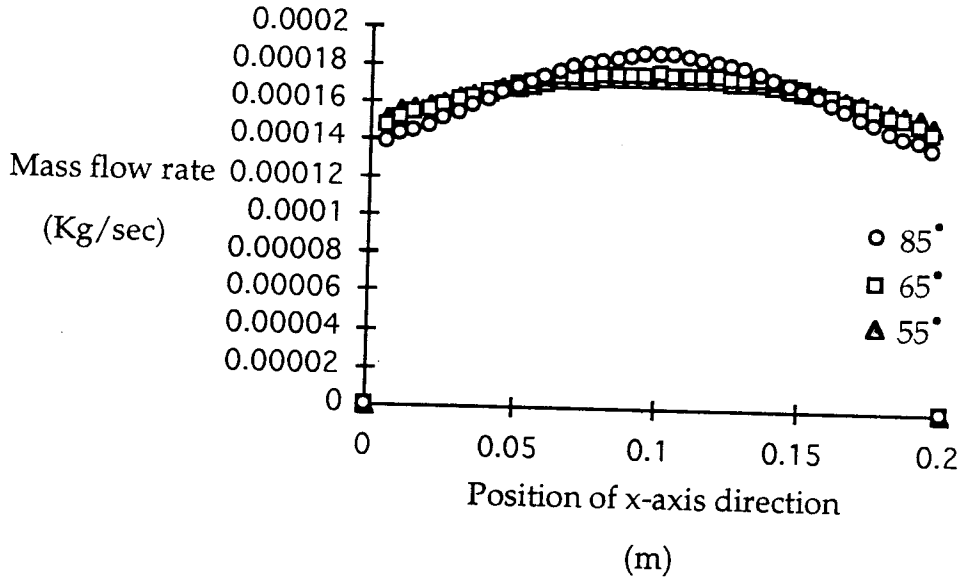

Figure 4.17 Flow rate distributions at the die exit for various manifold angles for $n = 0.6$.
$K = 10000\ Pa \cdot \sec$,
Length of Landing Zone $L = 0.05\ m$,
Inlet Velocity = 0.5 $m / \sec$

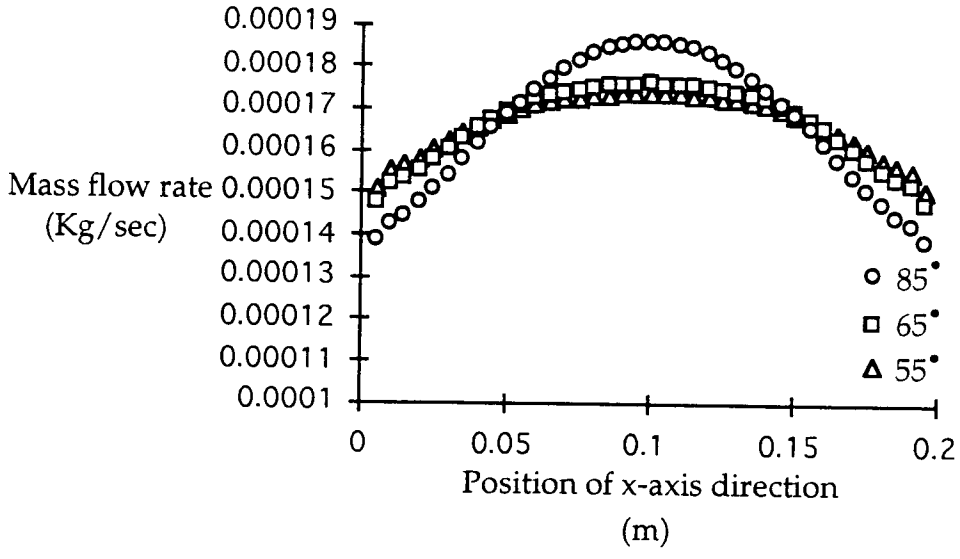

Figure 4.18 Flow rate distributions at the die exit for various manifold angles for n = 0.6. K = 10000 $Pa \cdot \sec$, Length of Landing Zone L = 0.05 m, Inlet Velocity = 0.5 $m / \sec$

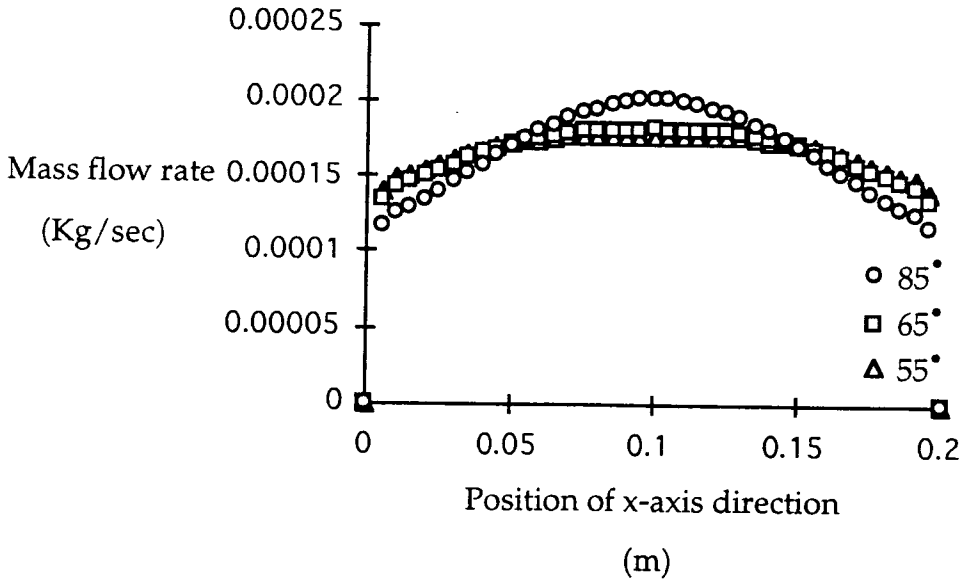

Figure 4.19 Flow rate distributions at the die exit for various manifold angles for n = 0.4.
K = 10000 $Pa \cdot \sec$,
Length of Landing Zone L = 0.05 m,
Inlet Velocity = 0.5 $m / \sec$

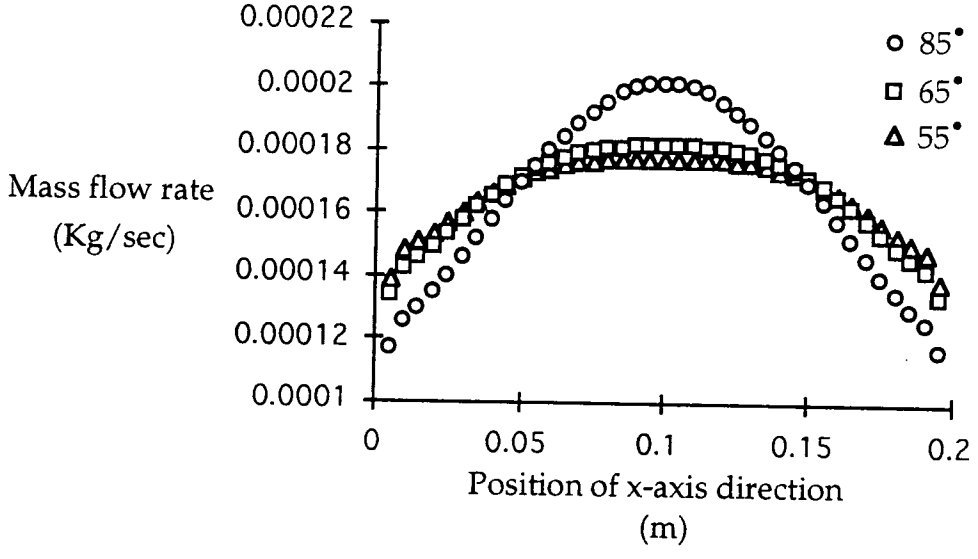

Figure 4.20 Flow rate distributions at the die exit for various manifold angles for $n = 0.4$.
$K = 10000\ Pa \cdot \sec$,
Length of Landing Zone $L = 0.05\ m$,
Inlet Velocity = 0.5 m / sec

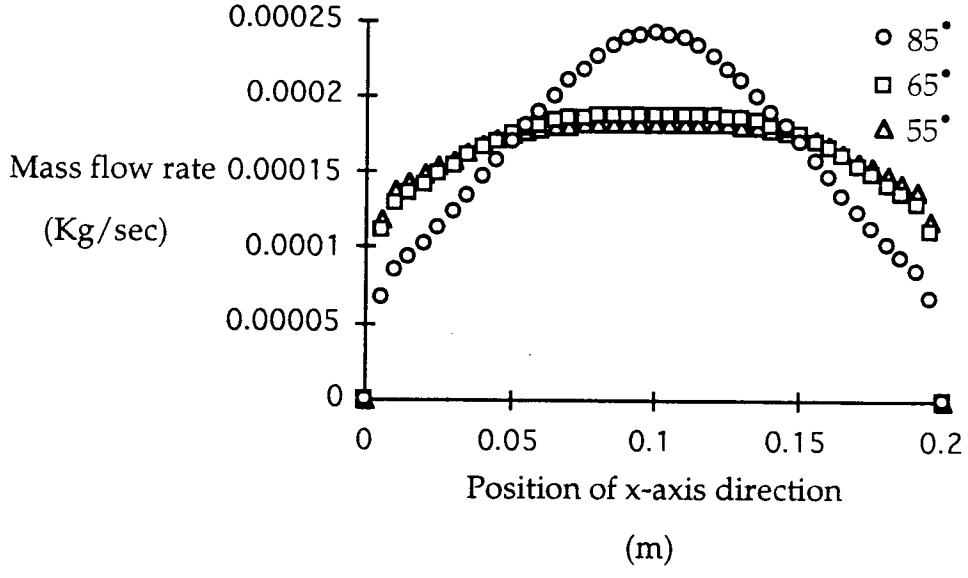

Figure 4.21 Flow rate distributions at the die exit for various manifold angles for $n = 0.2$.
$K = 10000\ Pa \cdot \sec$,
Length of Landing Zone $L = 0.05\ m$,
Inlet Velocity = 0.5 $m / \sec$

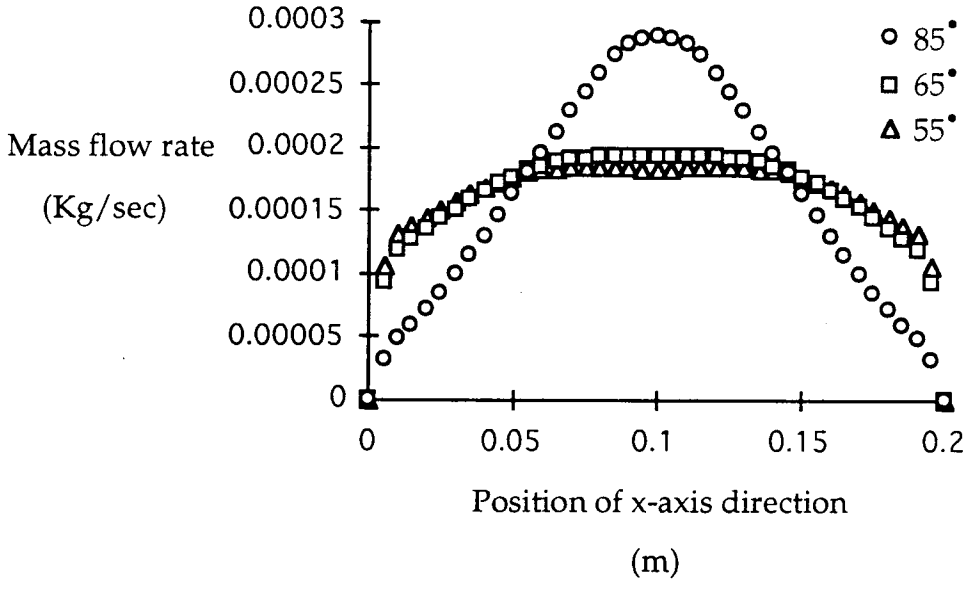

Figure 4.22 Flow rate distributions at the die exit for various manifold angles for $n = 0.12$.
$K = 10000\ Pa \cdot \sec$,
Length of Landing Zone $L = 0.05\ m$,
Inlet Velocity = 0.5 $m / \sec$

both valid and extremely crucial to obtaining uniform flow and a uniform film thickness. This was seen in Figure 4.5 of section 4.2, where the flow rate distribution at the exit of the die was given for the case of $n = 0.12$ with various manifold angles from $\theta = 85^\circ$ to $\theta = 55^\circ$. For this highly non-Newtonian case, the flow rate distribution was extremely sensitive to manifold angle, with a very distinct difference between the flow rate distributions in the ranges $\theta > 75^\circ$ and $\theta < 65^\circ$. *The capability to pick out this region and design around it is an important contribution of the flow simulations performed in this study.*

A summary of the simulation results for $n = 1.0$ to 0.12 is presented in Figure 4.23 for $\theta = 55^\circ$, Figure 4.24 for $\theta = 65^\circ$, and Figure 4.25 for $\theta = 85^\circ$. In these figures, the results have been normalized to the maximum mass flow rate for the y-axis and the die width for the x-axis. In these normalized dimensions, it is easy to pick out the fraction of the exit die width which is approximately at a uniform film thickness for each manifold angle. Using the criteria of a 10% deviation from the maximum allowed at the edges of the film, it can be seen in Figure 4.24 that even for the preferred case of $\theta = 65^\circ$ with a highly non-Newtonian fluid ($n = 0.12$), only the central 60% of the film will be of uniform thickness at the die exit. In a typical film extrusion process, the outer 10% of the film on each edge will be waste due to handling. This means that an additional 10% material on each edge will be waste loss due to processing. Therefore, it appears that the best that can be done even when optimizing the die geometry is to reduce the non-uniformity of film thickness at the die exit to minimize waste - but not completely eliminate it. This is the main reason that additional tools, such as adjustable die lips, are added to most commercial film dies.

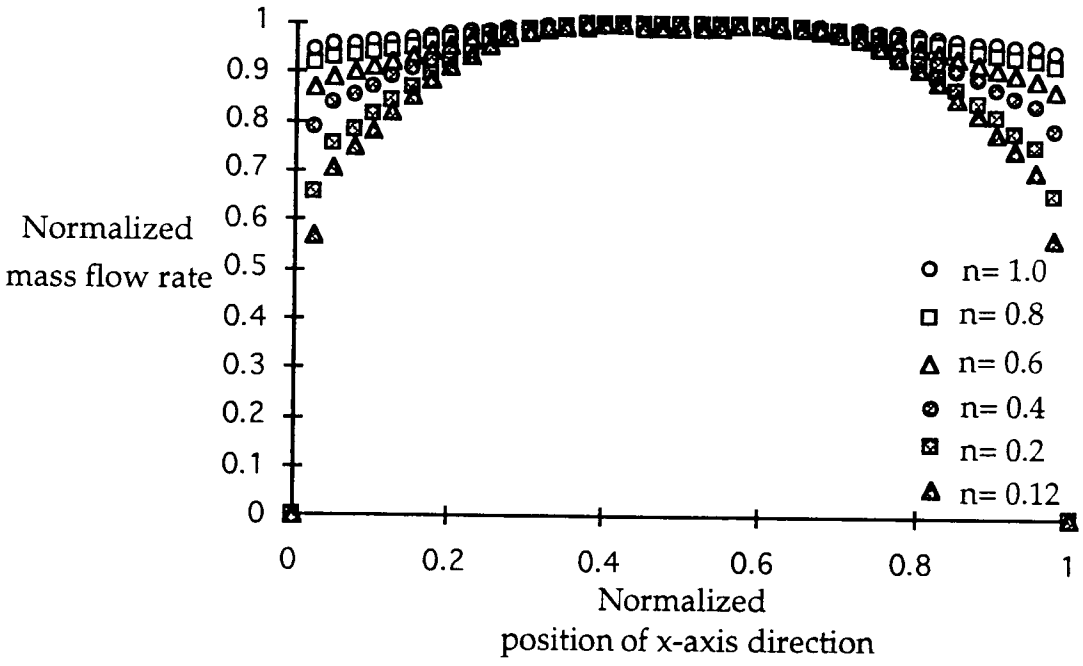

Figure 4.23 Normalized flow rate distributions at the die exit for various n values.
K = 10000 $Pa \cdot \sec$,
Manifold Angle θ = 55°,
Length of Landing Zone L = 0.05 m,
Inlet Velocity = 0.5 m / sec

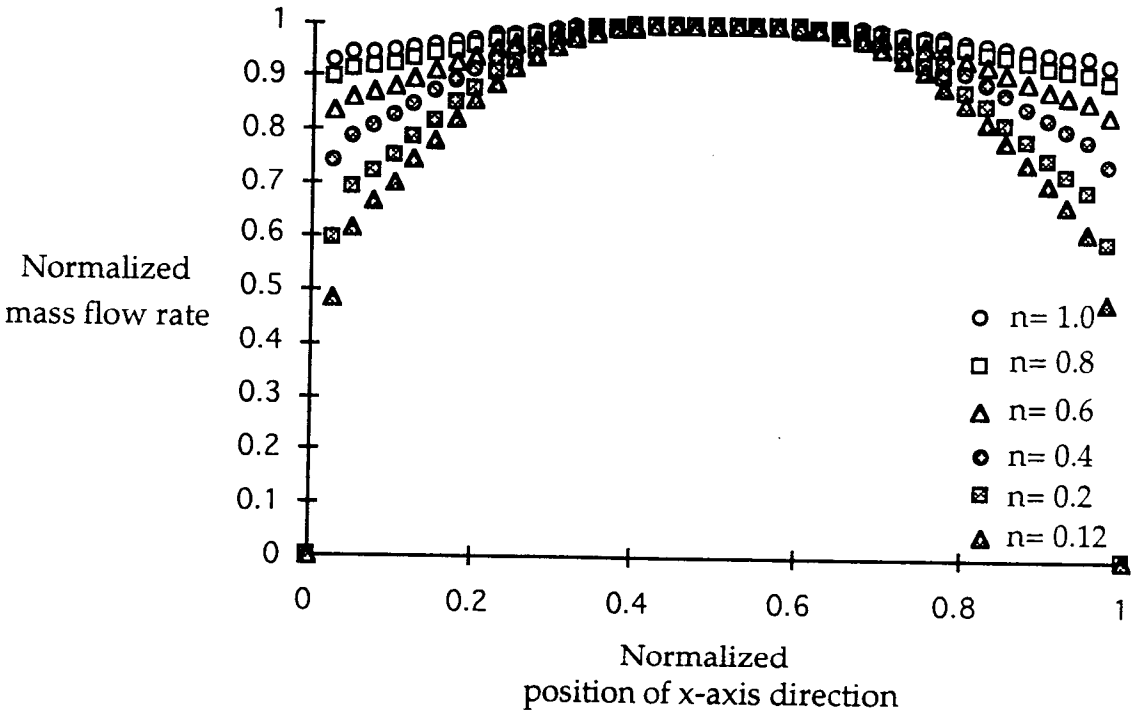

Figure 4.24 Normalized flow rate distributions at the die exit for various n values.
K = 10000 $Pa \cdot \sec$,
Manifold Angle $\theta = 65^{\circ}$,
Length of Landing Zone L = 0.05 m,
Inlet Velocity = 0.5 m / sec

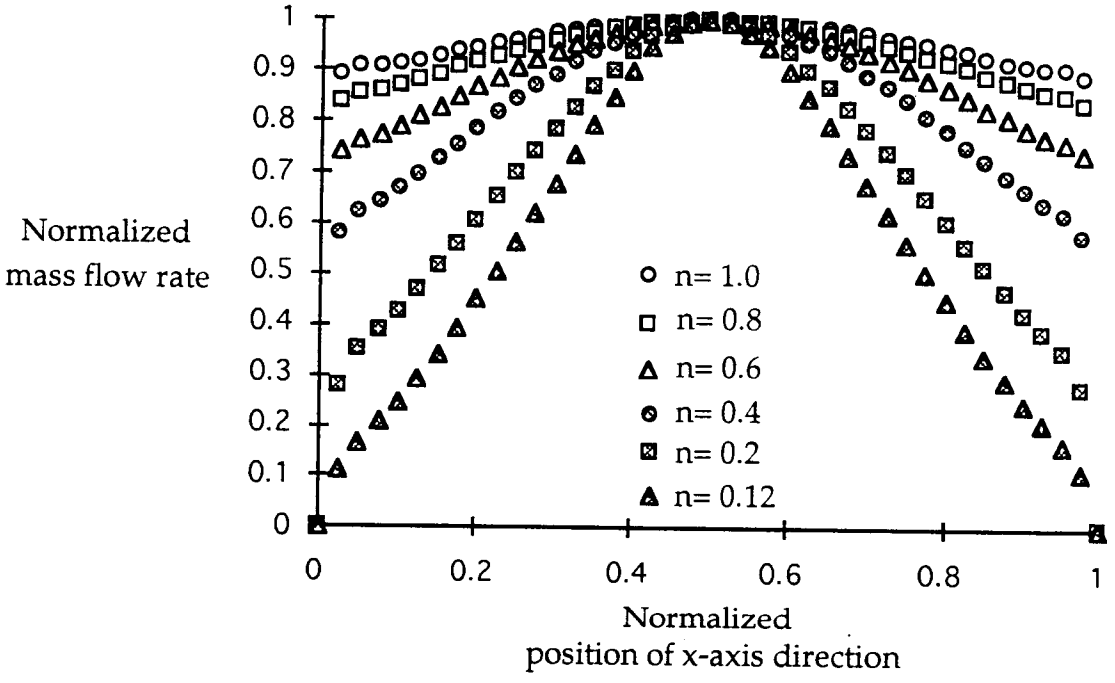

Figure 4.25 Normalized flow rate distributions at the die exit for various n values.
K = **10000** $Pa \cdot \sec$,
Manifold Angle θ = **85°**,
Length of Landing Zone L = **0.05** m,
Inlet Velocity = **0.5** $m / \sec$

In summary, it appears that the concept of a preferred manifold angle is extremely important to achieve final film uniformity in the cases where the material to be processed is highly non-Newtonian ($n < 0.5$). For materials that have power-law indices $n > 0.5$, the final film uniformity is fairly independent of manifold angle. However, it has also been shown that even for the case with an optimized manifold angle, for material with power-law indices around $n = 0.1$- 0.2, it is only possible to minimize waste due to non-uniform film thickness - not to eliminate it.

CHAPTER 5: SUMMARY, CONCLUSIONS AND RECOMMENDATIONS

5.1 Summary and conclusions

A Computational Fluid Dynamics (CFD) approach has been used to perform a parametric study to design a coathanger die for power-law fluids. A commercially available CFD program (FLUENT) which would be available for general use in an industrial setting was chosen for this purpose. The initial stimulus for the work came from the challenge of designing a film die for the production of high performance thin films from a lyotropic liquid crystal polymer system, poly (*p*-phenylene-cis-benzobisoxazole) in polyphosphoric acid (PBO/PPA). The rheological properties of the PBO/PPA system are high viscosity at low shear rate and highly non-Newtonian, shear-thinning behavior which can be described by the power-law model with a low value of the power-law index (n = 0.1 - 0.2) over the shear rate range of interest in the commercial film die.

From this specific application, the study was expanded to address the question of die design for power-law fluids in general. Based on previous analytical work by Chung and Lohkamp (1976), the main independent parameters studied to determine the preferred geometry of the film die were inlet velocity (or flow rate), length of the landing zone (L), and manifold angle (θ). The criteria used to determine the preferred geometry was uniform film thickness at the die exit (i.e., uniform flow rate across the width). A three-dimensional simulation with only two limiting assumptions, isothermal fluid flow and power-law fluid behavior (with n = 1.0 - 0.1), was developed. The most general results from the modeling show that die exit

film thickness uniformity is not strongly effected by inlet flow rate, but can be optimized as a function of manifold angle after determining the asymptotic region for the length of landing zone (L). The asymptotic region for the landing zone length is defined, in this study, as that length beyond which "entrance effects" are no longer significant. These entrance effects are a function of the length of prelanding zone, which is determined from the manifold angle (θ). Therefore, in practice the designer would typically determine the landing zone length based on criteria such as maximum allowable pressure drop through the die, then use the method outlined in this thesis to select the preferred manifold angle (θ), using uniform film thickness at the die exit as the performance criteria. The preferred manifold angle for a coathanger film die designed for the PBO/PPA system was $\theta = 65°$ for landing zone length $L = 0.05\ m$, inlet flow rate = 3.9270 m^3/sec, and power-law model parameters $K = 10000\ Pa \cdot \text{sec}$ and $n = 0.12$. It was determined that the optimized geometry was not very sensitive to the magnitude of the viscosity or to the power-law index for values of n > 0.5. However, for highly non-Newtonian fluids (n = 0.1 - 0.2) such as the PBO/PPA system, the flow distribution at the die exit was very sensitive to manifold angle.

Some of the details of the various parameters examined to obtain this result are summarized below.

(1) The specific die design that was studied was a linearly tapered coathanger die with a teardrop shaped manifold with cross-sectional angle = 60°. The various manifold angles that were examined ranged from $\theta = 55°$ to 85°. As was mentioned above, an preferred manifold angle was obtained for the particular case of the PBO/PPA system with the power-law parameters K = 10000 $Pa \cdot \text{sec}$ and $n = 0.12$, and was found to be $\theta = 65°$. Once this was

determined, a number of the parameters that were used to determine this manifold angle (n, K, and L) were varied to ensure that it was indeed an optimized value for a wide range of fluid and geometrical conditions.

(2) The effect of the landing zone length on the flow rate distribution at the die exit was examined for the manifold angle $\theta = 65^\circ$, the inlet flow rate = 3.9270 $m^3/\sec(w = 0.5 m/\sec)$, a power-law fluid with $K = 10000\ Pa \cdot \sec$, and n = 0.12, and the following lengths of landing zone; $L = 0.001\ m$, $0.01\ m$, $0.03 m$, $0.05\ m$, and $0.07\ m$. It was found that the die exit flow rate distribution became more uniform with increasing length of the landing zone (L), but that it appeared to be asymptotically approaching an optimum value near $L = 0.05$ m . It was obvious that a minimum L was needed to have something approaching a uniform die exit flow rate distribution, but that the determination of a preferred manifold angle was unaffected by the choice of the length of the landing zone. This result was consistent with what one might expect from looking at the coathanger die geometry and the expected flow from the manifold region (Figure 3.7). The preland length does not change dramatically with the manifold angle in the range $\theta = 55^\circ - 85^\circ$ (i.e., the preland length is not a strong function of θ). Therefore, the length of the landing zone to give a uniform mass flow rate distribution at the die exit should also not be a strong function of θ. Once the asymptotic value of the landing zone length (L) mentioned above was determined, it would not be expected to change dramatically for another manifold angle. It would most probably be more sensitive to fluid parameters, in particular the power-law index n. In a commercial application, there is a high priority placed on designing dies with a short landing zone length because this situation leads to lower pressure drop through the die, and consequently higher throughput. Choosing a landing zone length which is neither too short (which is

catastrophic due to the grossly uneven flow rate distribution) nor too long (which leads to high pressure drop and low throughput) is therefore a high priority, and can easily be done with 3-D simulations.

(3) The effect of inlet velocity (flow rate) was examined and found not to effect the selection of the preferred die geometry. The simulation was performed with the manifold angle $\theta = 82^\circ$ (predicted from the Equation 3.3) and the length of the landing zone $L = 0.05\ m$ when the inlet flow rates are $7.8540 \times 10^{-6}\ m^3/\sec$ ($w = 0.1\ m/\sec$), $1.5708 \times 10^{-5}\ m^3/\sec$ ($w = 0.2\ m/\sec$), $3.14159 \times 10^{-5}\ m^3/\sec$ ($w = 0.4\ m/\sec$), $4.71239 \times 10^{-5}\ m^3/\sec$ ($w = 0.6\ m/\sec$), and $6.28319 \times 10^{-5}\ m^3/\sec$ ($w = 0.8\ m/\sec$), where w is the average inlet velocity. The power-law data for the PBO/PPA solution ($\eta = K\dot{\gamma}^{n-1}$, K = 10000 $Pa \cdot \sec$, and n = 0.12) was used for the simulation. There was no value of the inlet flow rate at which the die had a relatively uniform film thickness distribution across the width.

(4) To examine the sensitivity of the simulation to the magnitude of the viscosity, the K value in the power-law model (consistency index) was varied (K = 1000, 5000, and 10000 $Pa \cdot \sec$) with various manifold angles ($\theta = 55^\circ$, 65°,and 85°). It was observed that there was virtually no effect of varying K value on the flow rate distribution for any manifold angle. This result is consistent with the predictions of Chung and Lohkamp (Equation 3.3), in which there is no predicted dependence of manifold angle on K value.

(5) The second important parameter in the power-law model is the power-law index (n), which determines the non-Newtonian nature of the fluid. In order to examine the sensitivity of the simulation to the value of the power-law index used, various n values were tested (n = 1.0, 0.8, 0.6, 0.4, 0.2, and 0.12) with various manifold angles ($\theta = 55^\circ, 65^\circ$,and 85°). There were several interesting observations that resulted from these simulations. First, for $n >$

0.5 there was very little effect on the flow rate distribution at the die exit, even for the largest manifold angle ($\theta = 85^\circ$). The implication is that for a fluid of moderate non-Newtonian character ($1.0 \geq n \geq 0.5$), there is essentially no preferred manifold angle; any manifold angle between $\theta = 55^\circ$ and $\theta = 85^\circ$ will give approximately uniform flow distribution at the die exit. However, for fluids that are highly non-Newtonian ($n < 0.5$), which includes many polymer melts and virtually all liquid crystal polymers (thermotropic or lyotropic), then the manifold angle chosen becomes important for obtaining a uniform flow rate distribution at the exit. For these highly non-Newtonian fluids, the concept of an preferred manifold angle is both valid and extremely crucial to obtaining uniform flow, and subsequently, a uniform film thickness.

5.2 Recommendations

There is really one major recommendation for future studies, and that relates to the choice of constitutive equation used to model the liquid crystal polymer. Generally speaking, polymer melts and solutions exhibit viscoelastic behavior during polymer processing. Even though the linear tapered coathanger film die is designed specifically to have smooth flow paths to minimize geometric perturbations which stimulate viscoelastic behavior, extrudate swell appears in most real polymer processes. These effects may in fact be minimized for the aligned and rigid liquid crystal polymers, particularly for anisotropic material at high temperatures where the viscosities are lower than for typical thermoplastic materials. However, LLCPs are known to exhibit anomalous flow behaviors and it would be reassuring to

repeat the optimization simulations for a variety of constitutive equations which would allow for the inclusion of viscoelasticity and yield stress ("gel like" behavior). Unfortunately, one of the limitations of the FLUENT code is that it does not allow for viscoelastic models, therefore another CFD package will be needed to perform these simulations. As was mentioned in the introduction, even the most general of CFD codes is usually still developed with some specialization. There are a few other CFD packages available which were developed specifically for use with non-Newtonian fluids in processing applications, and would have these capabilities. NEKTON (Fluent, Inc.) and POLYFLOW (POLYFLOW s.a., Belgium) are two which we are aware of that could be used for these simulations in the future.

BIBLIOGRAPHY

Arpin, B. and Lafleur, P. G., "Simulation of Polymer Flow through a Coat-Hanger Die: A Comparison of Two Numerical Approaches," *Polym. Eng. Sci.*, **32**, 206 (1992)

Arpin, B., Lafleur, P. G., and Sanschagrin, B., "A Personal Computer Software Program for Coathanger Die Simulation," *Polym. Eng. Sci.*, **34**, 657 (1994)

Charbonneaux, T. G., "Design of Sheet Dies for Minimum Residence Time Distribution: A Review," *Polym.-Plast. Technol. Eng.*, **30** (7), 665 - 684 (1991)

Chung, C. I. and Lohkamp, D. T., "Designing Coat-Hanger Dies by Power-Law Approximation," *Modern Plastics*, 52 (Mar.,1976)

Ernst, B., Denn, M. M., Pierini, P. E., and Rochefort, W. E., "Rheological properties of liquid crystalline solutions of poly(*p*-phenylene-cis-benzobisoxazole) in polyphosphoric acid (PBO/PPA)," *J. Rheol.*, **36** (2), (1992)

Ferry, J. D., **Viscoelastic Properties of Polymers**, Second Edition, John Wiley & Sons, New York (1960)

Hsu, T. C., Lichkus, A. M., and Harrison, I. R., "Liquid Crystal Polymer/Polyethylene Blends for Thin Film Applications," *Polym. Eng. Sci.*, **33**, 860 (1993)

Huebner, K. H. and Thornton, E. A., **The Finite Element Method for Engineers**, Second Edition, John Wiley & Sons, New York (1982)

James, D., Denn, M. M., Pierini, P., and Rochefort, W. E., "Capillary Rheometry of cis-PBO in Polyphosphoric Acid," submitted to *J. Rheol.*, (1995)

Lee, K.-Y., Wen, S.-H., and Liu, T.-J., "Vortex Formation in a Dual-Cavity Coat-Hanger Die," *Polym. Eng. Sci.*, **30**, 1220 (1990)

Liu, T.-J., Hong, C.-N., and Chen, K.-C., "Computer-Aided Analysis of Linearly Tapered Coat-Hanger Die," *Polym. Eng. Sci.*, **28**, 1517 (1988)

Matsubara, Y., "Geometry Design of a Coat-Hanger Die with Uniform Flow Rate and Residence Time Across the Die Width," *Polym. Eng. Sci.*, **19**, 169 (1979)

Matsubara, Y., "Design of Coat-Hanger Sheeting Dies Based on Ratio of Residence Times in Manifold and Slot," *Polym. Eng. Sci.*, **20**, 716 (1980)

Matsubara, Y., "Residence Time Distribution of Polymer Melts in the Linearly Tapered Coat-Hanger Die," *Polym. Eng. Sci.*, **23**, 17 (1983)

Mckelvey, J. M., **Polymer Processing**, John Wiley & Sons, New York (1962)

Mckelvey, J. M. and Ito, K., "Uniformity of Flow from Sheeting Dies," *Polym. Eng. Sci.*, **11**, 258 (1971)

Middleman, S., **Fundamentals of Polymer Processing**, McGraw-Hill, New York (1977)

Pearson, J. R. A., "Non-Newtonian Flow and Die Design," *Trans. J. Plastics Inst.*, **32**, 239 (1964)

Rauwendaal, C., "The Basics of Flat- Die Design," *Plastics World*, 61 (April, 1991)

Rauwendaal, C., "How proper die design can improve profile quality," *Plastics World*, 73 (Nov., 1991)

Roitman, D. B., Wessling, R.A., and McAlister, J., "Characterization of Poly(p-phenylene-cis-benzobisoxazole) in Methanesulfonic Acid,"*Macromolecules* , **26** (15), 4045 (1993a)

Roitman, D. B., Tung, L. H., Serrano, M., Wessling, R.A., and Pierini, P., "Polymerization Kinetics of Poly(*p*-phenylene-cis-benzobisoxazole), "*Macromolecules* , **26** (19), 5174 (1993b)

Samulski, E. T. and Dupre, D. B., **Advances in Liquid Crystals**, Academic Press. Inc., New York (1979)

Tadmor, Z. and Gogos, C. G., **Principles of Polymer Processing**, John Wiley & Sons, New York (1979)

Thomas, L. D. and Roth, D. D., "Film from Liquid Crystals," *CHEMTECH*, 546 (Sep.,1990)

Vergnes, B., Saillard, P., and Agassant, J. F., "Non-Isothermal Flow of a Molten Polymer in Coat-Hanger Die," *Polym. Eng. Sci.*, **24**, 980 (1984)

Wang, Y., "The Flow Distribution of Molten Polymer in Slit Dies and Coat-Hanger Dies Through Three-Dimensional Finite Element Analysis," *Polym. Eng. Sci.*, **31**, 204 (1991)

Winter, H. H. and Fritz, H. G., "Design of Dies for the Extrusion of Sheets and Annular Parisons: The Distribution problem," *Polym. Eng. Sci.*, **26**, 543 (1986)

APPENDICES

APPENDIX 1: FLUENT FIGURES

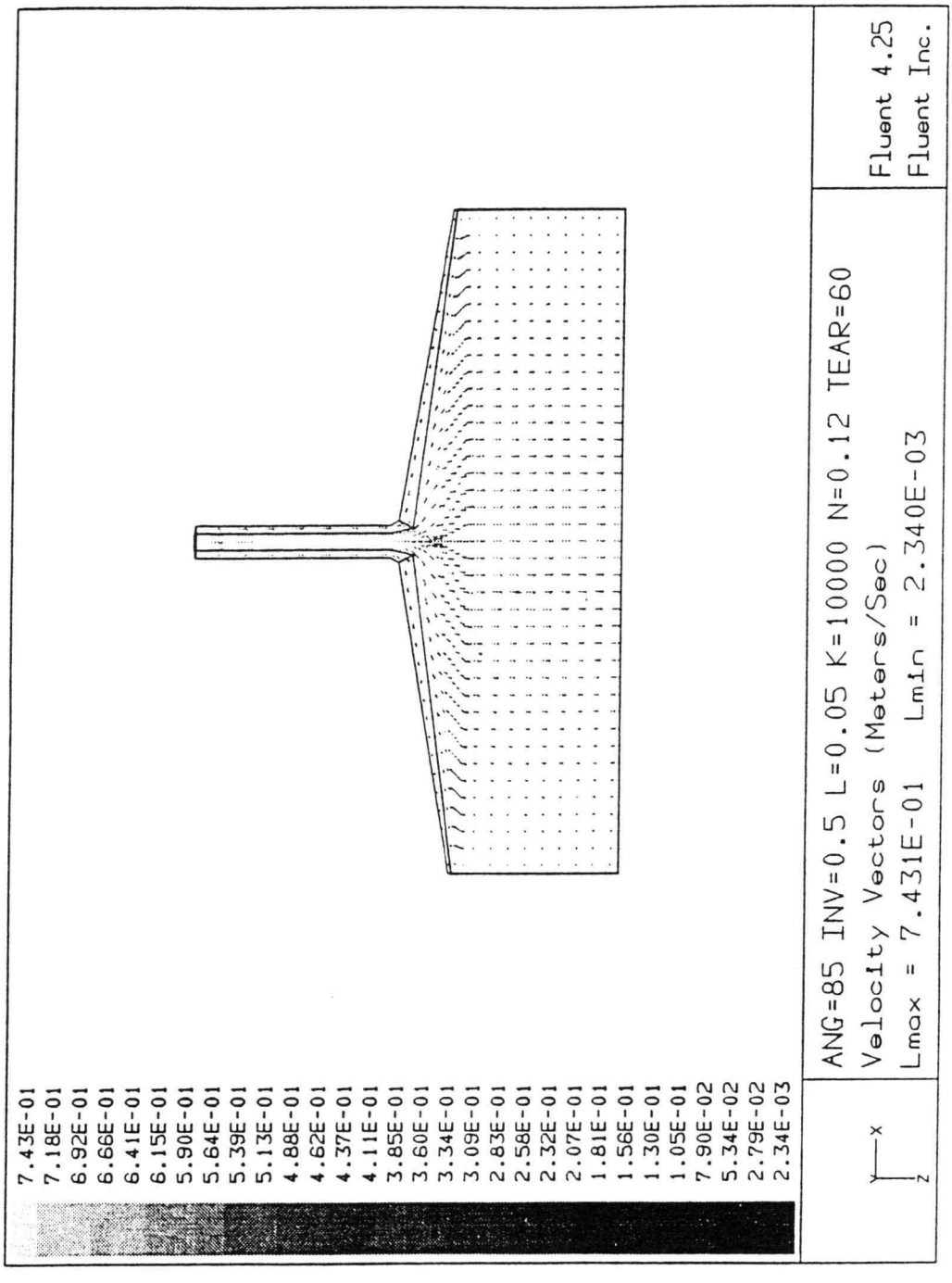

Figure 1.1 The plane view of velocity vectors on the center symmetry surface for $\theta = 85^{\circ}$. Power-Law Fluid ($K = 10000\ Pa \cdot \sec$; $n = 0.12$), Length of Landing Zone $L = 0.05\ m$, Inlet Velocity = $0.5\ m/\sec$

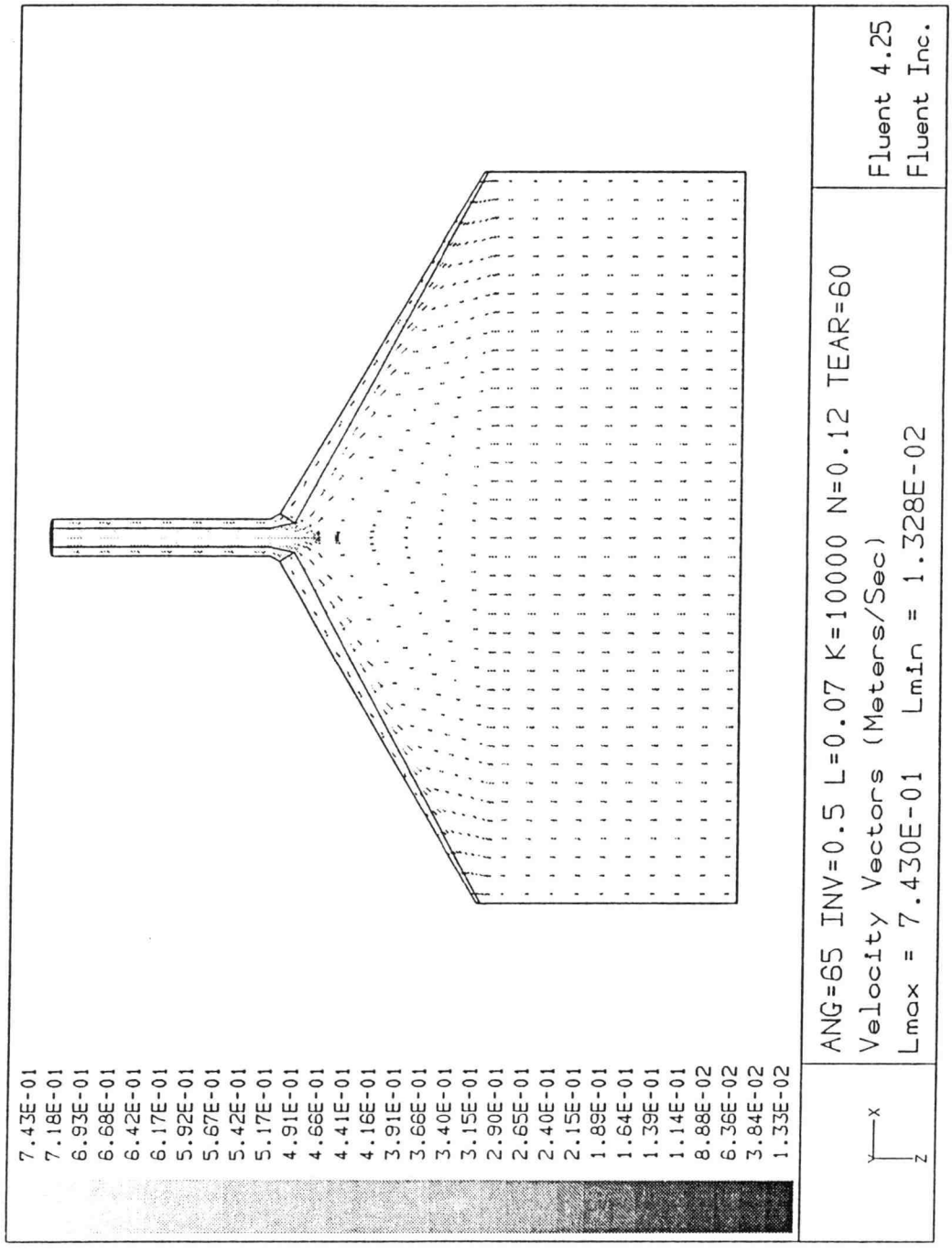

Figure 1.2 The plane view of velocity vectors on the center symmetry surface for $\theta = 65^{\circ}$. Power-Law Fluid ($K = 10000\ Pa \cdot \sec$; $n = 0.12$), Length of Landing Zone $L = 0.07\ m$, Inlet Velocity = $0.5\ m/\sec$

APPENDIX 2: RAW DATA

FLOW RATE DISTRIBUTION FOR VARIOUS INLET VELOCITIES					
K = 10000 Pa.sec		n = 0.12			
Manifold Angle = 82		Length of Landing Zone L = 0.05 m			
x-width	Mass flow rate (Kg/sec) for various inlet velocities				
(m)	0.1 m/sec	0.2 m/sec	0.4 m/sec	0.6 m/sec	0.8 m/sec
0	0	0	0	0	0
0.005	7.0833E-06	0.00001365	2.6617E-05	4.0867E-05	0.00005625
0.01	1.0673E-05	1.9773E-05	0.0000383	5.6717E-05	7.5717E-05
0.015	1.3275E-05	2.4983E-05	0.00004865	7.1817E-05	9.5333E-05
0.02	1.5953E-05	3.0817E-05	0.0000606	9.0067E-05	0.00011812
0.025	1.8797E-05	3.6767E-05	7.2967E-05	0.0001092	0.00014323
0.03	2.1783E-05	0.00004295	8.5433E-05	0.00012905	0.00017002
0.035	2.4833E-05	4.9817E-05	9.9767E-05	0.00014928	0.00019833
0.04	0.0000279	5.6383E-05	0.00011345	0.00016933	0.000225
0.045	3.0983E-05	6.3133E-05	0.00012785	0.0001896	0.0002525
0.05	3.4017E-05	6.9917E-05	0.00014172	0.00021	0.00028
0.055	3.6983E-05	7.5967E-05	0.00015397	0.00022983	0.000306
0.06	0.00003985	8.1817E-05	0.00016585	0.00024683	0.00032783
0.065	4.2517E-05	8.7133E-05	0.00017607	0.00026083	0.00034667
0.07	4.5033E-05	9.1717E-05	0.0001845	0.00027367	0.000365
0.075	4.7383E-05	9.5567E-05	0.00019132	0.00028567	0.000383
0.08	0.0000496	9.9417E-05	0.000199	0.00029883	0.00039967
0.085	5.1533E-05	0.00010307	0.00020617	0.00030883	0.00041167
0.09	0.0000523	0.000104	0.0002075	0.00031083	0.000414
0.095	5.2783E-05	0.00010418	0.00020717	0.00031117	0.0004145
0.1	0.000053	0.000104	0.00020617	0.00031083	0.000414

Table 2.1 data in section 4.1

FLOW RATE DISTRIBUTION FOR VARIOUS INLET VELOCITIES					
K = 10000 Pa.sec		n = 0.12			
Manifold Angle = 82		Length of Landing Zone L = 0.05 m			
x-width	Mass flow rate (Kg/sec) for various inlet velocities				
(m)	0.1 m/sec	0.2 m/sec	0.4 m/sec	0.6 m/sec	0.8 m/sec
0.105	5.2783E-05	0.00010363	0.00020567	0.00031017	0.00041317
0.11	0.0000523	0.00010325	0.00020483	0.00030933	0.00041167
0.115	5.1533E-05	0.00010217	0.00020333	0.000307	0.00040933
0.12	0.0000496	9.8517E-05	0.00019633	0.00029683	0.00039733
0.125	4.7383E-05	9.4283E-05	0.00018768	0.00028233	0.00038
0.13	4.5033E-05	9.0083E-05	0.00018033	0.00026917	0.00036133
0.135	4.2517E-05	8.5983E-05	0.00017228	0.00025667	0.00034283
0.14	3.9833E-05	8.1133E-05	0.00016365	0.00024433	0.00032533
0.145	3.6983E-05	7.5517E-05	0.00015268	0.0002295	0.0003055
0.15	3.4017E-05	6.9333E-05	0.00014027	0.000211	0.000282
0.155	3.0983E-05	6.2983E-05	0.00012713	0.00019032	0.00025483
0.16	0.0000279	5.6167E-05	0.00011273	0.00016988	0.00022733
0.165	2.4833E-05	4.9917E-05	9.9967E-05	0.00015128	0.0002015
0.17	2.1783E-05	4.3233E-05	0.00008615	0.00013103	0.00017383
0.175	1.8797E-05	0.0000365	7.2283E-05	0.0001112	0.00014758
0.18	1.5953E-05	3.0967E-05	6.1217E-05	0.00009315	0.00012335
0.185	1.3275E-05	2.5783E-05	0.00005085	7.6133E-05	0.00010078
0.19	1.0673E-05	2.0533E-05	0.0000404	6.1117E-05	8.1133E-05
0.195	7.0833E-06	1.4052E-05	2.7833E-05	0.00004385	0.0000601
0.2	0	0	0	0	0

Table 2.1 data in section 4.1 (continued)

FLOW RATE DISTRIBUTION FOR VARIOUS MANIFOLD ANGLES			
K = 10000 Pa.sec		n = 0.12	
Inlet Velocity = 0.5 m/sec		Length of Landing Zone L = 0.05 m	
x-Width (m)	Mass flow rate (Kg/sec) for various manifold angles (degree)		
	55	63	65
0	0	0	0
0.005	0.00010515	0.000095833	0.00009345
0.01	0.00013032	0.00012183	0.00011912
0.015	0.000138	0.00013028	0.00012807
0.02	0.00014477	0.00013798	0.00013578
0.025	0.0001512	0.0001455	0.00014367
0.03	0.00015742	0.00015317	0.00015137
0.035	0.00016312	0.00015997	0.00015887
0.04	0.00016842	0.00016638	0.00016565
0.045	0.00017265	0.0001719	0.00017153
0.05	0.00017633	0.00017685	0.00017685
0.055	0.00017927	0.00018107	0.00018125
0.06	0.0001818	0.00018403	0.00018477
0.065	0.00018327	0.00018677	0.0001877
0.07	0.00018402	0.00018878	0.00019008
0.075	0.00018473	0.00019007	0.00019173
0.08	0.00018473	0.00019098	0.00019267
0.085	0.00018453	0.00019102	0.00019317
0.09	0.00018378	0.00019097	0.00019317
0.095	0.00018325	0.00019097	0.00019317
0.1	0.00018325	0.00019097	0.00019317

Table 2.2 data in section 4.2

FLOW RATE DISTRIBUTION FOR VARIOUS MANIFOLD ANGLES K = 10000 Pa.sec n = 0.12 Inlet Velocity = 0.5 m/sec Length of Landing Zone L = 0.05 m			
x-Width (m)	Mass flow rate (Kg/sec) for various manifold angles (degree) 55	63	65
0.105	0.00018325	0.00019097	0.00019317
0.11	0.00018378	0.00019097	0.00019317
0.115	0.00018453	0.00019102	0.00019317
0.12	0.00018473	0.00019098	0.00019267
0.125	0.00018473	0.00019007	0.00019173
0.13	0.00018402	0.00018878	0.00019007
0.135	0.00018327	0.00018677	0.0001877
0.14	0.0001818	0.00018403	0.00018477
0.145	0.00017927	0.00018107	0.00018125
0.15	0.00017633	0.00017685	0.00017685
0.155	0.00017267	0.0001719	0.00017153
0.16	0.00016842	0.00016638	0.00016565
0.165	0.00016312	0.00015997	0.00015887
0.17	0.00015742	0.00015317	0.00015153
0.175	0.0001512	0.0001455	0.00014367
0.18	0.00014478	0.00013798	0.00013595
0.185	0.000138	0.00013028	0.00012807
0.19	0.00013065	0.00012185	0.00011912
0.195	0.00010533	0.000095833	0.000093467
0.2	0	0	0

Table 2.2 data in section 4.2 (continued)

FLOW RATE DISTRIBUTION FOR VARIOUS MANIFOLD ANGLES				
K = 10000 Pa.sec		n = 0.12		
Inlet Velocity = 0.5 m/sec Length of Landing Zone L = 0.05 m				
x-Width (m)	Mass flow rate (Kg/sec) for various manifold angles (degree)			
	66	75	82	85
0	0	0	0	0
0.005	9.0017E-05	0.00004735	3.7267E-05	0.000032133
0.01	0.00011622	7.0333E-05	4.8717E-05	0.00004815
0.015	0.00012537	0.0000853	6.1167E-05	0.00005955
0.02	0.0001338	9.9533E-05	0.00007595	0.000071333
0.025	0.0001422	0.00011342	0.00009155	0.000084633
0.03	0.00015043	0.00012763	0.00010775	0.000098633
0.035	0.00015813	0.00014097	0.00012562	0.00011343
0.04	0.0001651	0.00015392	0.00014277	0.0001293
0.045	0.00017135	0.00016617	0.00015992	0.00014553
0.05	0.00017687	0.0001775	0.00017653	0.00016232
0.055	0.0001818	0.0001881	0.00019187	0.00017912
0.06	0.00018567	0.0001975	0.0002065	0.000196
0.065	0.00018897	0.000206	0.00021867	0.00021233
0.07	0.00019153	0.00021333	0.000229	0.0002285
0.075	0.00019317	0.00021983	0.00023867	0.00024417
0.08	0.0001945	0.00022517	0.00024783	0.000259
0.085	0.00019517	0.000229	0.00025483	0.0002735
0.09	0.000195	0.00022983	0.00025567	0.00028117
0.095	0.00019517	0.00023117	0.00025517	0.00028583
0.1	0.00019517	0.00023167	0.000254	0.0002875

Table 2.2 data in section 4.2 (continued)

FLOW RATE DISTRIBUTION FOR VARIOUS MANIFOLD ANGLES				
K = 10000 Pa.sec		n = 0.12		
Inlet Velocity = 0.5 m/sec Length of Landing Zone L = 0.05 m				
x-Width (m)	Mass flow rate (Kg/sec) for various manifold angles (degree)			
	66	75	82	85
0.105	0.00019517	0.00023167	0.00025333	0.00028583
0.11	0.000195	0.0002315	0.00025333	0.00028117
0.115	0.00019517	0.00023133	0.00025233	0.0002735
0.12	0.0001945	0.00022717	0.00024567	0.000259
0.125	0.00019317	0.00022183	0.000236	0.00024417
0.13	0.00019153	0.00021517	0.00022583	0.0002285
0.135	0.00018897	0.0002075	0.0002155	0.00021233
0.14	0.00018567	0.00019883	0.0002045	0.000196
0.145	0.0001818	0.00018903	0.00019097	0.00017912
0.15	0.00017687	0.00017858	0.00017615	0.00016232
0.155	0.00017135	0.00016692	0.00016008	0.00014553
0.16	0.0001651	0.00015467	0.00014328	0.0001293
0.165	0.00015813	0.00014205	0.00012687	0.00011343
0.17	0.00015043	0.00012837	0.00010975	0.000098467
0.175	0.0001422	0.0001145	0.00009245	0.000084633
0.18	0.0001338	0.00010027	7.7117E-05	0.000071333
0.185	0.00012537	8.6017E-05	6.3883E-05	0.00005955
0.19	0.00011655	7.1033E-05	0.0000516	0.00004815
0.195	9.0017E-05	0.0000479	3.9267E-05	0.000032133
0.2	0	0	0	0

Table 2.2 data in section 4.2 (continued)

FLOW RATE DISTRIBUTION FOR VARIOUS LENGTHS OF LANDING ZONE					
K = 10000 Pa.sec		n = 0.12			
Manifold Angle = 65		Inlet Velocity = 0.5 m/sec			
x-width (m)	Mass flow rate (Kg/sec) for various lengths of landing zone (m)				
	0.001 m	0.01 m	0.03 m	0.05 m	0.07 m
0	0	0	0	0	0
0.005	0.00011592	0.00009345	3.7433E-05	5.3267E-06	1.178E-06
0.01	0.00013832	0.00011912	0.00006045	1.0537E-05	2.792E-06
0.015	0.00014255	0.00012807	7.9267E-05	1.9907E-05	6.635E-06
0.02	0.00014675	0.00013578	0.0000984	0.0000355	1.551E-05
0.025	0.00015117	0.00014367	0.00011735	5.8033E-05	3.303E-05
0.03	0.00015592	0.00015137	0.00013503	0.00008605	6.127E-05
0.035	0.00016033	0.00015887	0.00015128	0.00011713	0.0000983
0.04	0.0001649	0.00016565	0.00016605	0.00014848	0.0001392
0.045	0.00016877	0.00017153	0.00017903	0.00017788	0.0001792
0.05	0.00017225	0.00017685	0.0001902	0.00020437	0.0002145
0.055	0.00017537	0.00018125	0.00019967	0.00022667	0.0002428
0.06	0.00017828	0.00018477	0.00020733	0.00024417	0.0002633
0.065	0.00018032	0.0001877	0.00021317	0.00025667	0.0002772
0.07	0.00018182	0.00019008	0.0002175	0.0002645	0.000284
0.075	0.00018327	0.00019173	0.00022	0.00026717	0.0002843
0.08	0.0001842	0.00019267	0.00022083	0.00026567	0.0002787
0.085	0.00018492	0.00019317	0.0002195	0.00025817	0.0002655
0.09	0.00018528	0.00019317	0.0002155	0.00024467	0.0002452
0.095	0.00018547	0.00019317	0.00021383	0.00023933	0.0002373
0.1	0.00018565	0.00019317	0.00021383	0.00023867	0.0002367

Table 2.3 data in section 4.3

FLOW RATE DISTRIBUTION FOR VARIOUS LENGTHS OF LANDING ZONE					
K = 10000 Pa.sec		n = 0.12			
Manifold Angle = 65		Inlet Velocity = 0.5 m/sec			
x-width	Mass flow rate (Kg/sec) for various lengths of landing zone (m)				
(m)	0.001 m	0.01 m	0.03 m	0.05 m	0.07 m
0.105	0.00018547	0.00019317	0.00021383	0.00023933	0.0002373
0.11	0.00018528	0.00019317	0.0002155	0.00024467	0.000245
0.115	0.00018492	0.00019317	0.0002195	0.00025817	0.0002655
0.12	0.0001842	0.00019267	0.00022083	0.00026567	0.0002787
0.125	0.00018327	0.00019173	0.00022	0.00026717	0.0002843
0.13	0.00018182	0.00019007	0.0002175	0.00026433	0.000284
0.135	0.00018032	0.0001877	0.00021317	0.00025667	0.0002775
0.14	0.00017828	0.00018477	0.00020733	0.00024417	0.0002635
0.145	0.00017538	0.00018125	0.00019967	0.00022667	0.000243
0.15	0.00017243	0.00017685	0.0001902	0.00020418	0.0002145
0.155	0.00016877	0.00017153	0.00017903	0.00017788	0.0001791
0.16	0.0001649	0.00016565	0.00016605	0.00014848	0.0001392
0.165	0.00016033	0.00015887	0.00015128	0.00011713	0.0000983
0.17	0.00015592	0.00015153	0.00013503	8.6083E-05	6.132E-05
0.175	0.00015117	0.00014367	0.00011735	5.8083E-05	0.0000331
0.18	0.00014675	0.00013595	0.0000984	0.0000355	1.551E-05
0.185	0.00014255	0.00012807	7.9267E-05	1.9907E-05	6.638E-06
0.19	0.00013832	0.00011912	6.0517E-05	1.0537E-05	2.797E-06
0.195	0.00011592	9.3467E-05	3.7467E-05	5.3283E-06	1.178E-06
0.2	0	0	0	0	0

Table 2.3 data in section 4.3 (continued)

FLOW RATE DISTRIBUTION FOR VARIOUS K-VALUES K = 1000 Pa.sec n = 0.12 Length of Landing Zone = 0.05 m Inlet Velocity = 0.5 m/sec			
x-width (m)	Mass flow rate (Kg/sec) for various manifold angles(K=1000Pa.sec) 55 degree	65 degree	85 degree
0	0	0	0
0.005	0.00008495	0.0000729	0.000026467
0.01	0.00011615	0.00010223	0.0000399
0.015	0.0001284	0.00011538	0.000050883
0.02	0.00013862	0.00012672	0.00006295
0.025	0.00014777	0.0001375	0.000076283
0.03	0.00015617	0.00014773	0.000091033
0.035	0.00016385	0.00015723	0.00010672
0.04	0.0001706	0.00016583	0.00012383
0.045	0.00017612	0.00017335	0.000141
0.05	0.00018103	0.00018028	0.00015923
0.055	0.00018452	0.00018597	0.00017767
0.06	0.00018725	0.00019057	0.00019617
0.065	0.00018873	0.00019433	0.00021467
0.07	0.0001898	0.00019733	0.000233
0.075	0.00019015	0.00019917	0.00025083
0.08	0.00018962	0.0002005	0.00026867
0.085	0.0001885	0.00020117	0.000285
0.09	0.00018683	0.00020033	0.000294
0.095	0.00018612	0.00019983	0.00029933
0.1	0.0001861	0.0002	0.000301

Table 2.4 data in section 4.4

FLOW RATE DISTRIBUTION FOR VARIOUS K-VALUES K = 1000 Pa.sec n = 0.12 Length of Landing Zone = 0.05 m Inlet Velocity = 0.5 m/sec			
x-width (m)	Mass flow rate (Kg/sec) for various manifold angles(K=1000Pa.sec) 55 degree	65 degree	85 degree
0.105	0.00018612	0.00019983	0.0002995
0.11	0.00018683	0.00020033	0.000294
0.115	0.0001885	0.00020117	0.000285
0.12	0.00018978	0.0002005	0.00026867
0.125	0.00019017	0.00019917	0.000251
0.13	0.00018982	0.00019733	0.000233
0.135	0.0001889	0.0001945	0.00021467
0.14	0.00018725	0.00019073	0.00019633
0.145	0.00018453	0.00018597	0.00017783
0.15	0.00018103	0.0001803	0.00015923
0.155	0.00017628	0.00017335	0.000141
0.16	0.00017062	0.00016583	0.00012383
0.165	0.00016385	0.0001574	0.00010672
0.17	0.00015618	0.00014773	0.000091033
0.175	0.00014777	0.0001375	0.000076283
0.18	0.00013878	0.00012688	0.000062917
0.185	0.0001284	0.00011538	0.000050883
0.19	0.00011615	0.00010242	0.0000399
0.195	0.000084967	0.000072917	0.000026483
0.2	0	0	0

Table 2.4 data in section 4.4 (continued)

FLOW RATE DISTRIBUTION FOR VARIOUS K-VALUES K = 5000 Pa.sec n = 0.12 Length of Landing Zone = 0.05 m Inlet Velocity = 0.5 m/sec			
x-width (m)	Mass flow rate (Kg/sec) for various manifold angles(K=5000Pa.sec) 55 degree	65 degree	85 degree
0	0	0	0
0.005	0.000095733	0.000083683	0.000029583
0.01	0.00012485	0.00011222	0.000044483
0.015	0.00013453	0.00012265	0.0000557
0.02	0.00014225	0.00013232	0.000067667
0.025	0.00014975	0.0001413	0.000080983
0.03	0.00015688	0.00014973	0.0000952
0.035	0.0001633	0.00015813	0.00011068
0.04	0.00016917	0.00016565	0.00012658
0.045	0.00017412	0.00017243	0.0001437
0.05	0.00017832	0.0001783	0.00016087
0.055	0.00018178	0.00018325	0.00017857
0.06	0.00018398	0.00018747	0.000196
0.065	0.00018563	0.00019077	0.00021333
0.07	0.00018672	0.00019315	0.00023067
0.075	0.00018692	0.000195	0.00024733
0.08	0.00018673	0.00019617	0.00026333
0.085	0.00018617	0.00019667	0.00027867
0.09	0.00018505	0.00019633	0.000287
0.095	0.00018452	0.00019633	0.000292
0.1	0.0001845	0.00019633	0.00029367

Table 2.4 data in section 4.4 (continued)

FLOW RATE DISTRIBUTION FOR VARIOUS K-VALUES K = 5000 Pa.sec n = 0.12 Length of Landing Zone = 0.05 m Inlet Velocity = 0.5 m/sec			
x-width (m)	Mass flow rate (Kg/sec) for various manifold angles(K=5000Pa.sec) 55 degree	65 degree	85 degree
0.105	0.00018452	0.00019633	0.000292
0.11	0.00018505	0.00019633	0.000287
0.115	0.00018617	0.00019667	0.00027867
0.12	0.00018673	0.00019617	0.00026333
0.125	0.00018692	0.000195	0.00024733
0.13	0.00018672	0.00019315	0.00023067
0.135	0.00018563	0.00019077	0.00021333
0.14	0.000184	0.00018747	0.000196
0.145	0.00018178	0.00018325	0.00017857
0.15	0.00017832	0.0001783	0.00016087
0.155	0.00017412	0.00017243	0.0001437
0.16	0.00016917	0.00016565	0.00012658
0.165	0.0001633	0.00015813	0.00011068
0.17	0.00015688	0.00014973	0.0000952
0.175	0.00014977	0.0001413	0.000080983
0.18	0.00014225	0.00013232	0.000067667
0.185	0.00013453	0.00012265	0.0000557
0.19	0.00012485	0.00011222	0.000044483
0.195	0.000095733	0.000083717	0.000029583
0.2	0	0	0

Table 2.4 data in section 4.4 (continued)

FLOW RATE DISTRIBUTION FOR VARIOUS K-VALUES K = 10000 Pa.sec n = 0.12 Length of Landing Zone = 0.05 m Inlet Velocity = 0.5 m/sec			
x-width (m)	Mass flow rate (Kg/sec) for various manifold angles(K=10000Pa.sec) 55 degree	65 degree	85 degree
0	0	0	0
0.005	0.00010515	0.00009345	0.000032133
0.01	0.00013032	0.00011912	0.00004815
0.015	0.000138	0.00012807	0.00005955
0.02	0.00014477	0.00013578	0.000071333
0.025	0.0001512	0.00014367	0.000084633
0.03	0.00015742	0.00015137	0.000098633
0.035	0.00016312	0.00015887	0.00011343
0.04	0.00016842	0.00016565	0.0001293
0.045	0.00017265	0.00017153	0.00014553
0.05	0.00017633	0.00017685	0.00016232
0.055	0.00017927	0.00018125	0.00017912
0.06	0.0001818	0.00018477	0.000196
0.065	0.00018327	0.0001877	0.00021233
0.07	0.00018402	0.00019008	0.0002285
0.075	0.00018473	0.00019173	0.00024417
0.08	0.00018473	0.00019267	0.000259
0.085	0.00018453	0.00019317	0.0002735
0.09	0.00018378	0.00019317	0.00028117
0.095	0.00018325	0.00019317	0.00028583
0.1	0.00018325	0.00019317	0.0002875

Table 2.4 data in section 4.4 (continued)

FLOW RATE DISTRIBUTION FOR VARIOUS K-VALUES K = 10000 Pa.sec n = 0.12 Length of Landing Zone = 0.05 m Inlet Velocity = 0.5 m/sec			
x-width (m)	Mass flow rate (Kg/sec) for various manifold angles(K=10000Pa.sec) 55 degree	65 degree	85 degree
0.105	0.00018325	0.00019317	0.00028583
0.11	0.00018378	0.00019317	0.00028117
0.115	0.00018453	0.00019317	0.0002735
0.12	0.00018473	0.00019267	0.000259
0.125	0.00018473	0.00019173	0.00024417
0.13	0.00018402	0.00019007	0.0002285
0.135	0.00018327	0.0001877	0.00021233
0.14	0.0001818	0.00018477	0.000196
0.145	0.00017927	0.00018125	0.00017912
0.15	0.00017633	0.00017685	0.00016232
0.155	0.00017267	0.00017153	0.00014553
0.16	0.00016842	0.00016565	0.0001293
0.165	0.00016312	0.00015887	0.00011343
0.17	0.00015742	0.00015153	0.000098467
0.175	0.0001512	0.00014367	0.000084633
0.18	0.00014478	0.00013595	0.000071333
0.185	0.000138	0.00012807	0.00005955
0.19	0.00013065	0.00011912	0.00004815
0.195	0.00010533	0.000093467	0.000032133
0.2	0	0	0

Table 2.4 data in section 4.4 (continued)

FLOW RATE DISTRIBUTION FOR VARIOUS n-VALUES K = 10000 Pa.sec n = 1.0 (Newtonian Fluid) L=0.05m Inlet Velocity = 0.5 m/sec			
x-width (m)	Mass flow rate (Kg/sec) for various manifold angles(n=1.0) 55 degree	65 degree	85 degree
0	0	0	0
0.005	0.00016008	0.00015885	0.00015565
0.01	0.000162	0.00016093	0.00015758
0.015	0.00016237	0.0001613	0.00015812
0.02	0.00016307	0.00016202	0.00015935
0.025	0.00016377	0.00016307	0.00016025
0.03	0.00016448	0.00016378	0.00016183
0.035	0.0001652	0.00016485	0.00016325
0.04	0.0001659	0.00016557	0.0001645
0.045	0.00016678	0.00016678	0.00016608
0.05	0.00016732	0.0001675	0.0001675
0.055	0.00016785	0.0001682	0.00016857
0.06	0.00016838	0.00016875	0.0001698
0.065	0.00016892	0.00016927	0.0001707
0.07	0.0001691	0.0001698	0.00017175
0.075	0.00016945	0.00016998	0.00017228
0.08	0.0001698	0.0001705	0.000173
0.085	0.00016997	0.00017068	0.00017352
0.09	0.00016998	0.0001707	0.00017388
0.095	0.00016998	0.0001707	0.00017422
0.1	0.00016998	0.00017087	0.00017423

Table 2.5 data in section 4.5

FLOW RATE DISTRIBUTION FOR VARIOUS n-VALUES K = 10000 Pa.sec n = 1.0 (Newtonian Fluid) L=0.05m Inlet Velocity = 0.5 m/sec			
x-width (m)	Mass flow rate (Kg/sec) for various manifold angles(n=1.0)		
	55 degree	65 degree	85 degree
0.105	0.00016998	0.0001707	0.00017422
0.11	0.00016998	0.0001707	0.00017388
0.115	0.00016997	0.00017068	0.00017352
0.12	0.0001698	0.0001705	0.000173
0.125	0.00016945	0.00016998	0.00017228
0.13	0.0001691	0.0001698	0.00017175
0.135	0.00016892	0.00016927	0.0001707
0.14	0.00016838	0.00016875	0.0001698
0.145	0.00016785	0.0001682	0.00016857
0.15	0.00016732	0.0001675	0.0001675
0.155	0.00016678	0.00016678	0.00016608
0.16	0.0001659	0.00016557	0.0001645
0.165	0.0001652	0.00016485	0.00016325
0.17	0.00016448	0.00016378	0.00016183
0.175	0.00016377	0.00016307	0.00016025
0.18	0.00016307	0.00016202	0.00015935
0.185	0.00016237	0.0001613	0.00015812
0.19	0.000162	0.00016093	0.00015758
0.195	0.00016008	0.00015885	0.00015565
0.2	0	0	0

Table 2.5 data in section 4.5 (continued)

FLOW RATE DISTRIBUTION FOR VARIOUS n-VALUES K = 10000 Pa.sec n = 0.8 L=0.05m Inlet Velocity = 0.5 m/sec			
x-width (m)	Mass flow rate (Kg/sec) for various manifold angles(n=0.8)		
	55 degree	65 degree	85 degree
0	0	0	0
0.005	0.00015713	0.00015517	0.0001495
0.01	0.00015943	0.00015748	0.00015197
0.015	0.00016013	0.00015837	0.00015338
0.02	0.0001612	0.00015945	0.00015498
0.025	0.00016227	0.0001612	0.00015693
0.03	0.00016335	0.00016247	0.0001589
0.035	0.00016458	0.00016405	0.00016138
0.04	0.00016582	0.00016547	0.00016352
0.045	0.00016688	0.00016688	0.00016582
0.05	0.00016762	0.00016813	0.00016762
0.055	0.00016867	0.00016903	0.00016973
0.06	0.00016938	0.00016992	0.00017152
0.065	0.00016992	0.00017063	0.00017312
0.07	0.00017045	0.00017133	0.00017453
0.075	0.00017063	0.00017187	0.00017577
0.08	0.00017115	0.00017205	0.00017667
0.085	0.00017133	0.00017257	0.00017755
0.09	0.00017152	0.00017275	0.00017808
0.095	0.00017152	0.00017277	0.00017828
0.1	0.00017152	0.00017277	0.00017845

Table 2.5 data in section 4.5 (continued)

FLOW RATE DISTRIBUTION FOR VARIOUS n-VALUES K = 10000 Pa.sec n = 0.8 L=0.05m Inlet Velocity = 0.5 m/sec			
x-width (m)	Mass flow rate (Kg/sec) for various manifold angles(n=0.8) 55 degree	65 degree	85 degree
0.105	0.00017152	0.00017277	0.00017828
0.11	0.00017152	0.00017275	0.00017808
0.115	0.00017133	0.00017257	0.00017755
0.12	0.00017115	0.00017205	0.00017667
0.125	0.00017063	0.00017187	0.00017577
0.13	0.00017045	0.00017133	0.00017453
0.135	0.00016992	0.00017063	0.00017312
0.14	0.00016938	0.00016992	0.00017152
0.145	0.00016867	0.00016903	0.00016973
0.15	0.00016762	0.00016813	0.00016762
0.155	0.00016688	0.00016688	0.00016582
0.16	0.00016582	0.00016547	0.00016352
0.165	0.00016458	0.00016405	0.00016138
0.17	0.00016335	0.00016247	0.0001589
0.175	0.00016227	0.0001612	0.00015693
0.18	0.0001612	0.00015945	0.00015498
0.185	0.00016013	0.00015837	0.00015338
0.19	0.00015943	0.00015748	0.00015197
0.195	0.00015713	0.00015517	0.0001495
0.2	0	0	0

Table 2.5 data in section 4.5 (continued)

FLOW RATE DISTRIBUTION FOR VARIOUS n-VALUES K = 10000 Pa.sec n = 0.6 L=0.05m Inlet Velocity = 0.5 m/sec			
x-width (m)	Mass flow rate (Kg/sec) for various manifold angles(n=0.6) 55 degree	65 degree	85 degree
0	0	0	0
0.005	0.00015097	0.00014758	0.00013847
0.01	0.00015507	0.00015187	0.00014273
0.015	0.0001565	0.00015363	0.0001447
0.02	0.00015812	0.00015562	0.00014757
0.025	0.00016025	0.00015812	0.00015078
0.03	0.0001622	0.00016062	0.00015435
0.035	0.00016417	0.0001631	0.0001581
0.04	0.00016578	0.00016525	0.00016168
0.045	0.00016757	0.0001674	0.00016525
0.05	0.00016882	0.00016935	0.00016847
0.055	0.00017023	0.00017078	0.00017152
0.06	0.00017097	0.00017222	0.00017453
0.065	0.00017185	0.00017328	0.00017722
0.07	0.00017257	0.00017402	0.00017953
0.075	0.00017277	0.00017455	0.0001815
0.08	0.00017328	0.00017525	0.00018312
0.085	0.00017347	0.00017562	0.00018455
0.09	0.00017365	0.0001758	0.00018545
0.095	0.00017382	0.00017597	0.00018615
0.1	0.00017382	0.00017613	0.00018617

Table 2.5 data in section 4.5 (continued)

FLOW RATE DISTRIBUTION FOR VARIOUS n-VALUES K = 10000 Pa.sec n = 0.6 L=0.05m Inlet Velocity = 0.5 m/sec			
x-width (m)	Mass flow rate (Kg/sec) for various manifold angles(n=0.6) 55 degree	65 degree	85 degree
0.105	0.00017382	0.00017597	0.00018615
0.11	0.00017365	0.0001758	0.00018545
0.115	0.00017347	0.00017562	0.00018455
0.12	0.00017328	0.00017525	0.00018312
0.125	0.00017277	0.00017455	0.0001815
0.13	0.00017257	0.00017402	0.00017953
0.135	0.00017185	0.00017328	0.00017722
0.14	0.00017097	0.00017222	0.00017453
0.145	0.00017023	0.00017078	0.00017152
0.15	0.00016882	0.00016935	0.00016847
0.155	0.00016757	0.0001674	0.00016525
0.16	0.00016578	0.00016525	0.00016168
0.165	0.00016417	0.0001631	0.0001581
0.17	0.0001622	0.00016062	0.00015435
0.175	0.00016023	0.00015812	0.00015078
0.18	0.00015812	0.00015562	0.00014757
0.185	0.00015633	0.00015363	0.0001447
0.19	0.00015507	0.00015187	0.00014273
0.195	0.00015097	0.00014758	0.00013847
0.2	0	0	0

Table 2.5 data in section 4.5 (continued)

FLOW RATE DISTRIBUTION FOR VARIOUS n-VALUES K = 10000 Pa.sec n = 0.4 L=0.05m Inlet Velocity = 0.5 m/sec			
x-width (m)	Mass flow rate (Kg/sec) for various manifold angles(n=0.4)		
	55 degree	65 degree	85 degree
0	0	0	0
0.005	0.00013925	0.00013383	0.00011692
0.01	0.00014787	0.00014263	0.00012518
0.015	0.00015057	0.00014588	0.00012932
0.02	0.00015347	0.00014948	0.00013435
0.025	0.00015705	0.00015345	0.00013977
0.03	0.00016047	0.00015777	0.00014588
0.035	0.00016353	0.00016173	0.000152
0.04	0.00016625	0.00016533	0.00015795
0.045	0.00016893	0.00016857	0.00016388
0.05	0.00017108	0.00017128	0.00016947
0.055	0.00017272	0.0001738	0.00017487
0.06	0.00017398	0.00017578	0.00017957
0.065	0.00017507	0.00017757	0.00018425
0.07	0.00017595	0.00017867	0.00018855
0.075	0.0001765	0.00017957	0.000192
0.08	0.00017685	0.00018028	0.00019523
0.085	0.00017687	0.00018082	0.00019812
0.09	0.00017687	0.000181	0.00019973
0.095	0.00017687	0.00018102	0.00020098
0.1	0.00017687	0.00018118	0.00020118

Table 2.5 data in section 4.5 (continued)

FLOW RATE DISTRIBUTION FOR VARIOUS n-VALUES K = 10000 Pa.sec n = 0.4 L=0.05m Inlet Velocity = 0.5 m/sec			
x-width (m)	Mass flow rate (Kg/sec) for various manifold angles(n=0.4)		
	55 degree	65 degree	85 degree
0.105	0.00017687	0.00018102	0.00020098
0.11	0.00017687	0.000181	0.00019973
0.115	0.00017687	0.00018082	0.00019812
0.12	0.00017685	0.00018028	0.00019523
0.125	0.0001765	0.00017957	0.000192
0.13	0.00017595	0.00017867	0.00018855
0.135	0.00017507	0.0001774	0.00018425
0.14	0.00017398	0.00017578	0.00017957
0.145	0.00017272	0.0001738	0.00017487
0.15	0.00017108	0.00017128	0.00016947
0.155	0.00016893	0.00016857	0.00016372
0.16	0.00016625	0.00016533	0.00015795
0.165	0.00016353	0.00016172	0.000152
0.17	0.00016047	0.00015777	0.00014588
0.175	0.00015705	0.00015345	0.00013977
0.18	0.00015347	0.00014948	0.00013435
0.185	0.00015057	0.00014572	0.00012932
0.19	0.00014787	0.00014263	0.00012518
0.195	0.00013925	0.00013385	0.00011692
0.2	0	0	0

Table 2.5 data in section 4.5 (continued)

FLOW RATE DISTRIBUTION FOR VARIOUS n-VALUES K = 10000 Pa.sec n = 0.2 L=0.05m Inlet Velocity = 0.5 m/sec			
x-width (m)	Mass flow rate (Kg/sec) for various manifold angles(n=0.2) 55 degree	65 degree	85 degree
0	0	0	0
0.005	0.0001188	0.0001115	0.0000673
0.01	0.0001373	0.00012963	0.000084667
0.015	0.00014243	0.00013548	0.000093383
0.02	0.0001477	0.00014165	0.00010298
0.025	0.00015298	0.00014785	0.00011298
0.03	0.0001581	0.00015388	0.00012388
0.035	0.00016302	0.0001599	0.00013497
0.04	0.00016755	0.00016537	0.00014625
0.045	0.00017105	0.00017028	0.00015737
0.05	0.00017448	0.00017448	0.0001688
0.055	0.00017652	0.00017797	0.00017955
0.06	0.00017868	0.00018072	0.00018992
0.065	0.00017997	0.00018325	0.0002001
0.07	0.00018105	0.00018492	0.0002095
0.075	0.00018177	0.00018637	0.00021817
0.08	0.00018178	0.00018745	0.000226
0.085	0.00018178	0.000188	0.00023383
0.09	0.0001814	0.000188	0.00023783
0.095	0.0001814	0.00018818	0.0002405
0.1	0.0001814	0.00018818	0.00024133

Table 2.5 data in section 4.5 (continued)

FLOW RATE DISTRIBUTION FOR VARIOUS n-VALUES K = 10000 Pa.sec n = 0.2 L=0.05m Inlet Velocity = 0.5 m/sec			
x-width (m)	Mass flow rate (Kg/sec) for various manifold angles(n=0.2)		
	55 degree	65 degree	85 degree
0.105	0.0001814	0.00018818	0.0002405
0.11	0.0001814	0.000188	0.00023783
0.115	0.00018178	0.000188	0.00023383
0.12	0.00018178	0.00018745	0.000226
0.125	0.00018177	0.00018637	0.00021817
0.13	0.00018105	0.00018492	0.0002095
0.135	0.00017997	0.00018325	0.0002001
0.14	0.00017868	0.00018072	0.00018992
0.145	0.00017653	0.00017797	0.00017955
0.15	0.00017448	0.00017448	0.0001688
0.155	0.00017105	0.00017028	0.00015737
0.16	0.00016755	0.00016537	0.00014625
0.165	0.00016302	0.0001599	0.00013497
0.17	0.0001581	0.00015388	0.00012388
0.175	0.00015298	0.00014785	0.00011298
0.18	0.0001477	0.00014165	0.00010298
0.185	0.00014243	0.00013548	0.000093383
0.19	0.0001373	0.00012963	0.000084667
0.195	0.00011913	0.0001115	0.0000673
0.2	0	0	0

Table 2.5 data in section 4.5 (continued)

FLOW RATE DISTRIBUTION FOR VARIOUS n-VALUES K = 10000 Pa.sec n = 0.12 L=0.05m Inlet Velocity = 0.5 m/sec			
x-width (m)	Mass flow rate (Kg/sec) for various manifold angles(n=0.12) 55 degree	65 degree	85 degree
0	0	0	0
0.005	0.00010515	0.00009345	0.000032133
0.01	0.00013032	0.00011912	0.00004815
0.015	0.000138	0.00012807	0.00005955
0.02	0.00014477	0.00013578	0.000071333
0.025	0.0001512	0.00014367	0.000084633
0.03	0.00015742	0.00015137	0.000098633
0.035	0.00016312	0.00015887	0.00011343
0.04	0.00016842	0.00016565	0.0001293
0.045	0.00017265	0.00017153	0.00014553
0.05	0.00017633	0.00017685	0.00016232
0.055	0.00017927	0.00018125	0.00017912
0.06	0.0001818	0.00018477	0.000196
0.065	0.00018327	0.0001877	0.00021233
0.07	0.00018402	0.00019008	0.0002285
0.075	0.00018473	0.00019173	0.00024417
0.08	0.00018473	0.00019267	0.000259
0.085	0.00018453	0.00019317	0.0002735
0.09	0.00018378	0.00019317	0.00028117
0.095	0.00018325	0.00019317	0.00028583
0.1	0.00018325	0.00019317	0.0002875

Table 2.5 data in section 4.5 (continued)

FLOW RATE DISTRIBUTION FOR VARIOUS n-VALUES K = 10000 Pa.sec n = 0.12 L=0.05m Inlet Velocity = 0.5 m/sec			
x-width (m)	Mass flow rate (Kg/sec) for various manifold angles(n=0.12) 55 degree	65 degree	85 degree
0.105	0.00018325	0.00019317	0.00028583
0.11	0.00018378	0.00019317	0.00028117
0.115	0.00018453	0.00019317	0.0002735
0.12	0.00018473	0.00019267	0.000259
0.125	0.00018473	0.00019173	0.00024417
0.13	0.00018402	0.00019007	0.0002285
0.135	0.00018327	0.0001877	0.00021233
0.14	0.0001818	0.00018477	0.000196
0.145	0.00017927	0.00018125	0.00017912
0.15	0.00017633	0.00017685	0.00016232
0.155	0.00017267	0.00017153	0.00014553
0.16	0.00016842	0.00016565	0.0001293
0.165	0.00016312	0.00015887	0.00011343
0.17	0.00015742	0.00015153	0.000098467
0.175	0.0001512	0.00014367	0.000084633
0.18	0.00014478	0.00013595	0.000071333
0.185	0.000138	0.00012807	0.00005955
0.19	0.00013065	0.00011912	0.00004815
0.195	0.00010533	0.000093467	0.000032133
0.2	0	0	0

Table 2.5 data in section 4.5 (continued)

APPENDIX 3: DERIVATION OF Equation 3.3

Equation 3.3 was derived by Chung and Lohkamp (1976) using the lubrication theory. In this section, brief description of the derivation of this equation is presented.

For a power-law fluid, the relationship between viscosity and shear rate is,

$$\eta = K\dot{\gamma}^{n-1} \qquad \text{Equation 1.1}$$

From the assumptions 3 to 5 in the section 3.6, the flow rate along the manifold for an isothermal power-law fluid can be expressed by the below equation (Figure 1.3).

$$Q(x) = \left(\frac{n\pi}{3n+1}\right)\cdot\left(\frac{1}{2K}\right)^{1/n}\left(R(x)^{(3n+1)/n}\right)\cdot\left(-\frac{dP(x)}{dx}\right)^{1/n} \qquad \text{Equation 1.2}$$

The flow rate per unit width of the coathanger die is given as,

$$S = \frac{Q_o}{W} \qquad \text{Equation 1.3}$$

where Q_o is the total flow rate. And S can be expressed in terms of the height of prelanding zone H_1 and the pressure gradient for an isothermal power-law fluid.

$$S = \frac{1}{2}\left(\frac{n}{2n+1}\right)\cdot\left(\frac{1}{2K}\right)^{1/n}\cdot\left(H_1^{(2n+1)/n}\right)\cdot\left(-\frac{dP(z)}{dz}\right)^{1/n} \qquad \text{Equation 1.4}$$

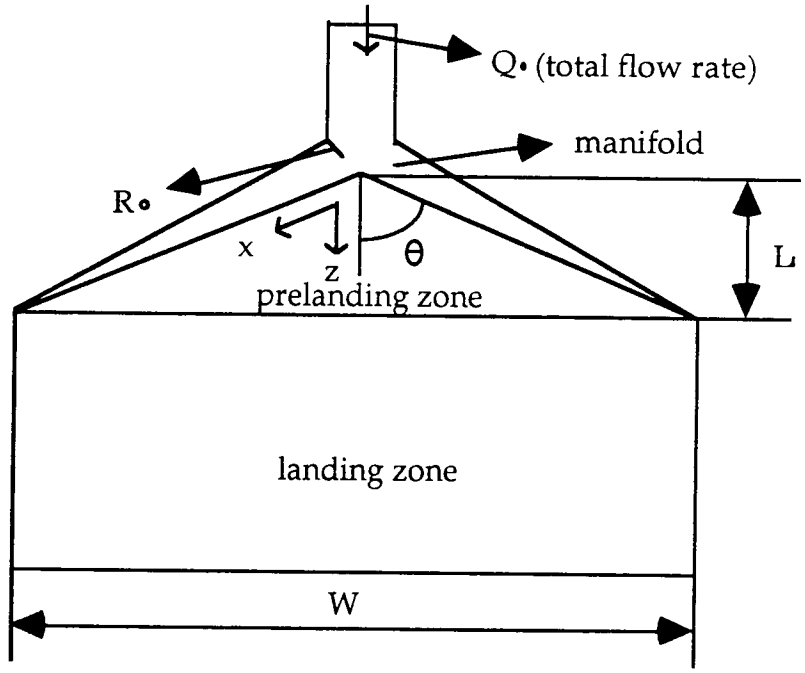

Figure 1.3 Coathanger die, component sections and flow axes (x, z)

where $x = \frac{z}{\cos\theta}$ Equation 1.5

Because S is independent of z (constant circular cross-section) and constant, the $\frac{-dP(z)}{dz}$ term in Equation 1.4 also must be constant.

$$\frac{-dP(z)}{dz} = \frac{\Delta P_1}{L_1} \qquad \text{Equation 1.6}$$

where L_1 is the length of prelanding zone and ΔP_1 is the pressure drop over the prelanding zone.

Inserting Equation 1.6 into Equation 1.4 leads to,

$$S = \frac{1}{2}\left(\frac{n}{2n+1}\right)\cdot\left(\frac{1}{2K}\right)^{1/n}\cdot\left(H_1^{(2n+1)/n}\right)\cdot\left(\frac{\Delta P_1}{L_1}\right)^{1/n} \qquad \text{Equation 1.7}$$

From the assumption 3 in the section 3.6, the pressure must be equal in the traverse direction. Thus, the pressure gradient along the manifold also must be constant.

$$\frac{-dP(x)}{dx} = \frac{\Delta P_1}{L_1}\cdot\cos\theta \qquad \text{Equation 1.8}$$

Inserting Equation 1.8 into Equation 1.2 gives

$$Q(x) = \left(\frac{n\pi}{3n+1}\right)\cdot\left(\frac{1}{2K}\right)^{1/n}\left(R(x)^{(3n+1)/n}\right)\cdot\left(\frac{\Delta P_1}{L_1}\cdot\cos\theta\right)^{1/n} \qquad \text{Equation 1.9}$$

Combining Equation 1.3 and Equation 1.7 gives,

$$\Delta P_1 = \left(\frac{Q_\circ}{W} \cdot \frac{1}{\left(n\pi/3n+1\right)\cdot\left(1/2K\right)^{1/n}}\right)^n \cdot \left(\frac{L_1}{H_1^{(2n+1)}}\right) \qquad \text{Equation 1.10}$$

The flow rate entering the manifold $Q(x)$ at $x=0$ is $\frac{Q_\circ}{2}$. The initial radius of the manifold can be expressed as $R_\circ$ at $x=0$. Inserting Equation 1.9 into Equation 1.10 for ΔP_1 gives,

$$R_\circ = \left[\frac{(3n+1)}{4\pi(2n+1)}W\right]^{\frac{n}{(3n+1)}}\left[\frac{H_1^{\frac{(2n+1)}{(3n+1)}}}{\cos\theta^{\frac{1}{(3n+1)}}}\right] \qquad \text{Equation 1.11}$$

which is Equation 3.3 of section 3.6.